Effects of *rok1* gene deletion on mitosis in fission yeast at appropriate and stressful temperatures and the molecular mechanisms

JIAYI HE[1*], MENGNAN LIU[1*], JIANI XU[1*], XIANG DING[2] and YILING HOU[1]

[1]Key Laboratory of Southwest China Wildlife Resources Conservation, Ministry of Education, College of Life Science, China West Normal University, Nanchong, Sichuan 637009, P.R. China; [2]Nanchong Key Laboratory of Eco-Environmental Protection and Pollution Control in Jialing River Basin, College of Environmental Science and Engineering, China West Normal University, Nanchong, Sichuan 637009, P.R. China

Received June 26, 2025; Accepted December 16, 2025

DOI: 10.3892/etm.2026.13145

Abstract. The *rok1* gene encodes the ATP-dependent RNA helicase Rok1, which is involved in regulating the maturation of small subunit ribosomal RNA and thus ribosome biogenesis. However, the regulation of cellular mitotic dynamics by the *rok1* gene deletion is currently unclear. In the present study, fluorescent protein labeling and live cell imaging techniques were used to investigate the effects of *rok*1 deletion on the dynamics of microtubules, actin and kinetochores during mitosis at 25 and 37˚C, and RNA-sequencing and bioinformatics analyses were used to reveal the key genes. Analysis of the live cell imaging results revealed that, in mitosis, the initiation length and contraction length of actin rings were both shortened and the contraction rate was decreased at 25 and 37˚C. The separation process of kinetochores was inhibited at 25 and 37˚C, and the inhibition was more severe at the higher temperature of 37˚C. Analysis of RNA sequencing results showed that upregulation of *myo51* and *blt1* resulted in delayed actin ring assembly and slowed actin ring contraction in the *rok1*Δ strain. In addition, *psm1* and *psc3* were upregulated and are key genes affecting the ability of kinetochores to move on the spindle and the cohesion of sister chromatids. The present study revealed that the Rok1 protein not only influences the actin polymerization process, participate in the regulation of actin ring assembly and contraction, and cytoplasmic division, but also affects the migration ability of kinetochores on the spindle and participate in the regulation of the formation and maintenance of cohesion between sister chromatids, which provides a certain scientific basis for further exploring the function of the Rok1 protein in cell division.

Correspondence to: Professor Xiang Ding, Nanchong Key Laboratory of Eco-Environmental Protection and Pollution Control in Jialing River Basin, College of Environmental Science and Engineering, China West Normal University, 1 Shida Road, Nanchong, Sichuan 637009, P.R. China
E-mail: biostart8083@126.com

Professor Yiling Hou, Key Laboratory of Southwest China Wildlife Resources Conservation, Ministry of Education, College of Life Science, China West Normal University, 1 Shida Road, Nanchong, Sichuan 637009, P.R. China
E-mail: starthlh@126.com

*Contributed equally

Key words: Schizosaccharomyces pombe, *rok1* gene, high-temperature stress, mitosis, RNA-sequencing

Introduction

The course of the eukaryotic cell cycle is regulated by genes and accompanied by periodic fluctuations in the expression levels of a number of genes (1). Maintaining cell cycle homeostasis requires coordinated interactions between proteins such as tubulin (2), actin (3) and cellular structures. Cell cycle dysregulation leads to genomic instability which leads to cell death, diseases and malignancies, such as breast cancer (4), esophageal cancer (5), and head and neck squamous cell carcinoma (6,7). *Schizosaccharomyces pombe* (*S. pombe*) is a eukaryotic organism with well-defined cell shapes and highly active homologous recombination mechanisms, making it a high-quality model organism in biology (8,9). The growth of fission yeast cells is susceptible to environmental changes; in conditions such as high temperatures or nutritional deficiencies, cells trigger a stress response that regulates cell cycle checkpoints to delay or arrest the mitotic process, disrupting cell cycle homeostasis (10). For example, when fission yeast cells are cultured at a suitable temperature (such as 25˚C), protein function in the cells is normal; however, when cultured at higher temperatures (such as 37˚C), protein function during mitosis is disturbed and cell cycle homeostasis is destroyed (11,12).

Almost all aspects of eukaryotic gene expression and its regulation involve ATP-dependent RNA helicases. The DEAD box protein family of RNA helicases is a key regulator of RNA splicing, mRNA export and ribosome biosynthesis. Mutations and dysregulation of the DEAD box protein family

have been associated with a variety of diseases, such as cancer and neurological disorders (13). The ATP-dependent RNA helicase Fal1 of the *S. pombe* DEAD box protein family is involved in the constitution of the exon junction complex subunit that recognizes and degrades mis-spliced mRNAs in the nucleus during the cell cycle. The *fal1* gene deletion results in the formation of ascus with more or fewer than four spores and abnormal mitosis (14,15). Ste13 has ATP-dependent histone chaperone activity that regulates the involvement of histone chaperones in chromatin assembly and de-assembly. The *ste13* mutant cannot enter the G_0 phase of the cell cycle or initiate sexual reproduction to produce spores (16). Dbp2 has RNA helicase activity and binds ATP and mRNA; it is involved in the composition of the ribonucleoprotein complex and regulates ribosome biogenesis. Deletion of the *dbp2* gene results in reduced localization of proteins to chromatin and mitotic cell cycle abnormalities (15). Translation initiation RNA helicase, Ded1, has translation initiation factor activity. In response to stress, Ded1 inhibits the activity of the Cdc25 protein in mitosis and activates the mitotic G_2/M checkpoint; however, under high temperature conditions, *ded1* mutant cells are unable to enter S phase and mitotic processes (11,17). Prp19 complex WD repeat protein Prp5, which is involved in the composition of the Prp19 complex, regulates DNA repair, recombination and spore formation, but at high temperatures, *prp5* mutations result in abnormal cell morphology, defective cell cycle proteins and cell cycle arrest at mitosis or the G_2/M border (18,19). The *uap56* gene encodes the TREX complex subunit, ATP-dependent RNA Uap56, which is involved in the mRNA metabolic process by catalyzing the attachment of RNA fragments through the spliceosome. Under high temperature conditions, the mitotic cell cycle of the *uap56*Δ strain is abnormal (15).

The *rok1* gene encodes the ATP-dependent RNA helicase Rok1 in *S. pombe*, which is a member of the DEAD box protein family (Fig. 1). In cells, the Rok1 protein is localized in the nucleolus and is involved in regulating the maturation of small subunit ribosomal RNA (rRNA) and thus the process of ribosome biogenesis (20). In budding yeast, the Rok1 protein binds to ATP, stabilizes the binding of its cofactor Rrp5 to the 40S ribosome (21) and is involved in rRNA processing and control of cell cycle progression in budding yeast (22). In fission yeast, *rok1* gene deletion results in decreased cell growth under high-temperature conditions and in media with galactose, maltose, sucrose or xylose as the carbon source, increased growth in media with lysine, proline or serine as the nitrogen source and increased susceptibility to bleomycin, brefeldin A, cycloheximide, diamide, formamide and sodium dodecyl sulfate. Abnormal chromosome segregation during meiosis was also observed in *rok1Δ* cells (23). In addition, the *rok1* gene is closely associated with human diseases, and Rok1 and Cd168 accelerate the progression of androgen-independent (AI) prostate cancer and accelerate the invasion and metastasis of AI cells in the endothelial layer of human bone marrow (24).

To the best of our knowledge, the effects of fission yeast *rok1* gene deletion on cell mitosis under normal and stress temperature conditions and its molecular mechanisms have not been reported. In the present study, the effects of *rok1* gene deletion on cell growth, sporulation and spindle, actin, kinetochores and centromere protein dynamics in mitosis were investigated using the fission yeast as a research model. RNA-sequencing (RNA-Seq) and bioinformatics analyses also revealed key genes and pathways of the abnormal growth of the *rok1Δ* strain, providing a scientific basis for further revealing the role of Rok1 protein in cell division.

Materials and methods

Experimental strains. The strains used in the present study are listed in Table I (25,26). All strains constructed in this experiment were engineered with fluorescent labels via spore production, as later described.

Culture media and main reagents. YE5S Liquid Medium was prepared by adding 2.5 g Yeast Extract (Thermo Fisher Scientific, Inc.), 0.01125 g Amino Acids (Ade/Leu/Ura/His/Lys) (Merck KGaA), 15 g Dextrose (Shanghai Aladdin Biochemical Technology Co., Ltd.) and 500 ml ultrapure Water. YE5S Solid Medium was prepared by adding 8.5 g agar (BioFroxx; neoFroxx GmbH) to the liquid medium. G418, HygR or NatMx Resistance Selection Medium were prepared by adding 0.3 mg/ml G418 (Guangzhou Saigou Biotech Co., Ltd.), 0.3 mg/ml HygR (Shanghai Macklin Biochemical Co., Ltd.) or 0.1 mg/ml NatMx (Beijing Solarbio Science & Technology Co., Ltd.) to YE5S solid medium. Leu-deficient medium was prepared by removing Leu from YE5S solid medium. 1X snail enzyme solution was prepared by mixing 100X snail enzyme buffer with 10 g/ml snail enzyme (Shanghai Yuanye Bio-Technology Co., Ltd.) and 990 μl ultrapure water. The 100X Snail Enzyme Buffer contains 1 mol/l sorbitol (Shanghai Yuanye Bio-Technology Co., Ltd.), 100 mmol/l EDTA (Shanghai Macklin Biochemical Co., Ltd.) and 14 mmol/l β-mercaptoethanol (Merck KGaA). All media and reagents were prepared at room temperature and sterilized prior to use.

Fluorescent protein labeling construction. The wild-type strain with fluorescent marker (PT2514, PT3850, YL20, YL24, YL26) and the opposite mating-type *rok1*Δ strain (2125-A or 2125-B) (Table I) were inoculated onto YE5S solid medium and were activated at 25˚C for 3 days. The activated h^+ and h^- strains were then mixed on EMM-N nitrogen-deficient medium for sporulation (27) and incubated at 25˚C for 2 days. Colonies were picked and examined using an OLYMPUS BX51 microscope (Olympus Corporation) to monitor sporulation. Upon confirmation of spore formation, the cells were treated with 1 ml prepared 1X snail enzyme working solution (28,29) to release the spore suspension. The suspension was spread onto YE5S solid medium and incubated at 25˚C for 2 days to allow spore germination and single colony formation. Colonies were subsequently transferred using the replica plating method onto nutrient-deficient or antibiotic-containing media (30). Positive clones obtained were expanded through serial passages, stored with 30% glycerol as cryoprotectant in an 80˚C ultra-low temperature freezer (Thermo Fisher Scientific, Inc.) for future use.

Live cell imaging. Live cell imaging of the experimental strains was performed using a TCS-SP8 laser confocal microscope (Leica Microsystems GmbH) at 25 and 37˚C. The parameters were set as follows: Green fluorescence received in the wavelength range of 493-545 nm, red fluorescence received in the

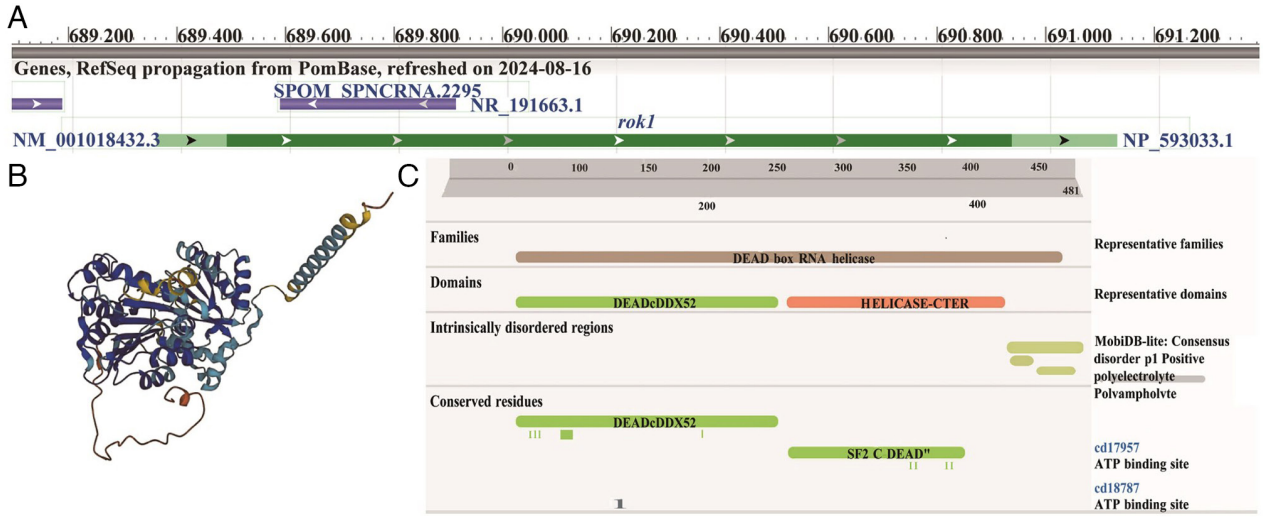

Figure 1. Location, protein structure and protein conserved domain of *rok1*. (A) Location of *rok1*. (B) Structure of the Rok1 protein. (C) Conserved domains of the Rok1 protein.

wavelength range of 584-736 nm, pixels of 512x512 μm, seven optical slices with a pitch of 6.02 μm, exposure time of 400 msec, shooting interval of 2 min and total shooting time of 120 min.

Outlier detection. Measurements of the dynamics of cellular mitotic spindle, actin, kinetochore, and centrosome proteins were analyzed using ImageJ (version 1.51s; National Institutes of Health). Potential outliers were identified and excluded based on the Z-score method. The Z-score was calculated as $Z=(\chi-\mu)/\sigma$, where χ is the measured value, μ is the mean of measurements and σ is the population standard deviation. Data points with Z>2 were considered outliers (31). To ensure data consistency across all metrics including microtubule, actin, kinetochore and centrosomal protein data, each initially collected from 20 cells (No. 1-No. 20), if a cell was identified as an outlier in any metric, all measurement data from that cell were excluded.

For example, using actin ring data from *rok1*Δ strains cultured at 25˚C, six metrics were analyzed: Actin ring length, total time from assembly to complete disappearance, assembly time, contraction time, total contraction rate from assembly to complete disappearance and contraction rate during the contraction phase. After Z-score normalization of measurements from the 20 cells, three outliers (Z>2) were identified: The contraction rate of the No. 4 cell and both the total duration and assembly time of the actin ring of the No. 14 cell. Consequently, all six parameters from the No. 4 and the No. 14 cells were excluded. Following this procedure, data from 5 cells were excluded for each metric, ultimately retaining a uniform set of 15 cells per metric for subsequent analysis.

Statistical analysis. Data analysis was performed using SPSS Statistics 26 (International Business Machines Corporation). The Shapiro-Wilk test assessed data normality, and the unpaired Student's t-test analyzed differences between wild-type and *rok1Δ* strains. Differentially expressed genes were identified using an adjusted P<0.05, $\log_2$ fold change >0 (32) as screening criteria. RT-qPCR data were analyzed using the $2^{-\Delta\Delta Cq}$ relative quantification method (33) to describe the transcriptional expression changes of target genes in the *rok1*Δ strain relative to the wild-type strain. P<0.05 was considered to indicate a statistically significant difference.

RNA-Seq. The PT287 and 2125 strains were cultured at 25˚C and 37˚C until the cells entered the logarithmic growth phase, and then the organisms were collected and frozen. Total RNA was extracted using the Yeast total RNA kit (Omega Bio-Tek, Inc.) according to the manufacturer's standard protocol, and sent to Beijing Novogene technology Co., Ltd. for quality testing and RNA-Seq. Reference genes were compared using Hisat2 v2.0.5 software (34); gene expression was quantified using Feature Counts and Stringtie (1.3.3b) software (35); and differential significance of gene expression of samples was analyzed using DESeq2 (1.20.0) and EdgeR (3.22.5) software (36). Differential genes were processed by Gene Ontology (GO) function enrichment (37), Kyoto Encyclopedia of Genes and Genomes (KEGG) (38) pathway enrichment analysis was performed using Cluster Profile software (version 3.8.1) (39).

Reverse transcription-quantitative PCR (RT-qPCR). PT287 and 2125 strains were cultured at 25 and 37˚C until the cells reached the logarithmic growth phase, then collected and frozen. Total RNA was extracted using the Yeast Total RNA Kit and reverse-transcribed into cDNA using the RevertAid First Strand cDNA Synthesis Kit (Thermo Fisher Scientific, Inc.) at 42˚C for 60 min. The qPCR conditions were as follows: 95˚C pre-denaturation for 30 sec, followed by 39 cycles of 95˚C denaturation for 5 sec and 60˚C annealing/extension for 30 sec. The melting curve analysis stage consisted of 95˚C for 10 sec, 65˚C for 5 sec and 95˚C for 5 sec. The *act1* gene was used as the internal control, and qPCR was performed using the CFX96 Real-Time PCR Detection System (Bio-Rad Laboratories, Inc.) to analyze gene expression levels. The primer sequences used are listed in Table II.

Table I. Strains and genotypes used in the present study.

Strain	Genotype	Source
PT286	h⁻ wt	Lab of Tran[a]
PT287	h⁺ wt	Lab of Tran[a]
PT2514	h⁻ Mis12-GFP:Leu/mC-Atb2:HygR	Lab of Tran[a]
PT3850	h⁺ Pact1-LifeAct-mGFP:LEU1	Lab of Tran[a]
YL20	h⁻ Sid4-GFP:NatMX/mC-Atb:HygR	Ding Zhang (25)
YL24	h⁻ mC-Atb2:HygR/Cut11-GFP :HygR	Ding Zhang (25)
YL26	h[b] GFP-Atb2:HygR/Hht1-RFP:HygR	Yu *et al* (26)
2125-A	h⁺ *rok1Δ*:kanR	Lab of Tran[a]
2125-B	h⁻ *rok1*Δ:kanR	Lab of Tran[a]
2125-1	h[b] *rok1*Δ:KanR/Mis12-GFP:Leu/mC-Atb2:HygR	Present study
2125-2	h[b] *rok1*Δ:KanR/Pact1-LifeAct-mGFP:LEU1	Present study
2125-3	h[b] *rok1*Δ:KanR/Sid4-GFP:NatMX/mC-Atb:HygR	Present study
2125-4	h[b] *rok1*Δ:KanR/mC-Atb2:HygR/Cut11-GFP :HygR	Present study
2125-5	h[b] *rok1*Δ:KanR/GFP-Atb2:HygR/Hht1-RFP:HygR	Present study

[a]Laboratory of Associate Professor Phong Tran. [b]The sex of yeast strain was not identified. GFP, green fluorescent protein; RFP, red fluorescent protein; wt, wild-type.

Table II. Primer sequences used for quantitative PCR.

Gene	Forward primer (5'→3')	Reverse primer (5'→3')
psc3	CGTTCAGCCTCAAGAACGGA	AATTGCGATACGAGCTAGGC
psm1	ATCAACGCTGAGTTACGCCA	CTAACTGCGCAGAGTCTCGT
myo51	TCGGTAGGCTCGGAATGTTG	AAGGCGACTCTGATTGACCG
blt1	TGACGGTTCATCCATCGTTT	ACTGGGCGTTTTCGTCTTCT
act1	CCCAAATCCAACCGTGAGAAG	CCAGAGTCCAAGACGATACC AGTG

Results

Changes in cell growth and spore production in the rok1Δ strain. The growth rates of the wild-type strain and the *rok1*Δ strain were compared and the results showed that there was no significant difference in growth rates between the two over the period of 0-4 h at 25˚C and 37˚C (all P>0.05). After 6 h, the wild-type strain entered the logarithmic growth phase and the growth rate of the *rok1*Δ strain significantly decreased. At 25˚C, optical density $(OD)_{595}$ at 12 h was 0.68±0.00 and 0.33±0.02 for the wild-type and *rok1*Δ strains, respectively. At 37˚C, OD_{595} at 12 h was 0.89±0.01 and 0.61±0.07 for the wild-type and *rok1*Δ strains, respectively (Fig. 2A and B), which were significantly different (P<0.01). The aforementioned results indicated that *rok1* gene deletion significantly decreased the cell growth rate.

The results of spore number production showed that 99.33±0.31% of the wild-type strains produced 4 spores, whereas the percentage of the *rok1*Δ strain producing 4 spores was 96.60±0.92%, which was a significant difference. In addition, there were 2.00±0.72% of the *rok1*Δ strain producing 3 spores (Fig. 2C and D). The results showed that the *rok1*Δ strain produced an abnormal number of spores compared to the wild-type strain, with a significant decrease in the number of spores. It is noteworthy that the high temperature of 37˚C significantly impacts spore production. Previous studies have reported that at 37˚C, gene-deleted fission yeast either fail to produce spores or exhibit a low probability of spore formation (40). Therefore, spore production was investigated exclusively at 25˚C.

A significant decrease in the growth rate of the *rok1*Δ strain was found by growth rate measurements; therefore, the mitosis-related protein dynamics of the *rok1*Δ strain was investigated.

Changes of spindle during mitosis of rok1Δ strain under different temperature conditions. During mitosis, microtubule proteins assemble to form the spindle, which is responsible for the accurate segregation of chromosomes during cell division (41). Live-cell imaging of wild-type and *rok1*Δ cells with green fluorescent protein (GFP)-Atb2-tagged microtubule proteins was used to assess spindle properties. The analysis of spindle dynamics at 25˚C showed that the spindle elongation lengths of the wild-type strains at the prophase, metaphase

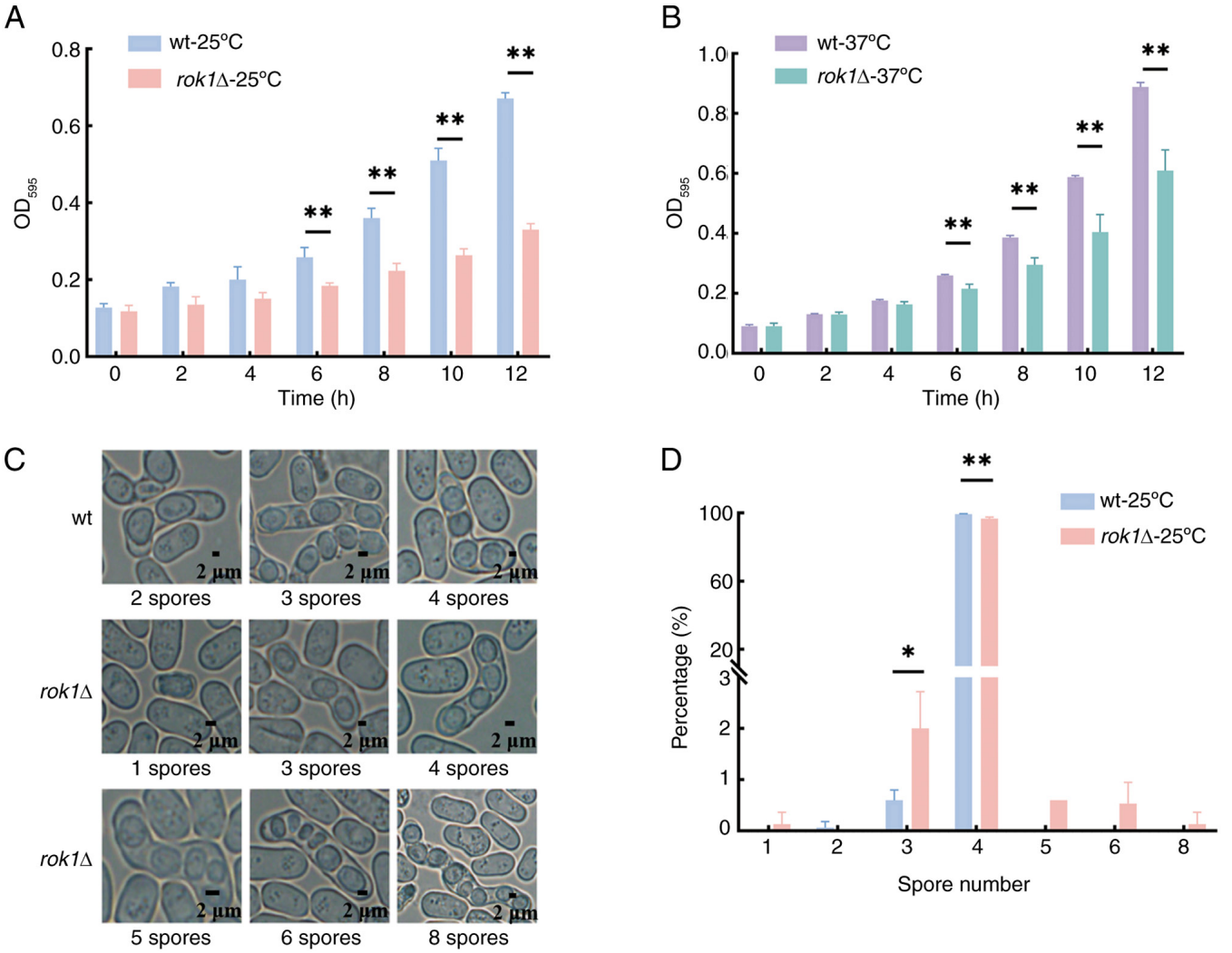

Figure 2. Effects of *rok1* deletion on cell growth and ascospores. (A) Growth rate analysis of wt and *rok1*Δ strains at 25˚C. (B) Growth rate analysis of wt and *rok1*Δ strains at 37˚C. (C) Spore morphology of wt and *rok1*Δ strains at 25˚C. (D) Number of spores in wt and *rok1*Δ strains. *P<0.05 and **P<0.01; n=1,200. wt, wild-type; OD, optical density.

and anaphase were 0.68±0.27, 0.63±0.23 and 8.82±0.62 μm and for the *rok1*Δ strain they were 0.75±0.22, 0.61±0.19 and 8.57±0.80 μm, respectively (Fig. 3A-D). The *rok1*Δ strain exhibited no significant changes in spindle elongation length compared to the wild-type strain in all phases (all P>0.05). Further analysis revealed (Fig. 3E and F) that the spindle elongation times of the wild-type strains at prophase, metaphase and anaphase were 3.33±1.45, 4.80±1.47 and 11.07±1.03 min and for the *rok1*Δ strain they were 4.27±1.83, 5.07±1.67 and 10.40±1.12 min, respectively. The spindle elongation rates of the wild-type and *rok1*Δ strains at the prophase, metaphase and anaphase were 0.22±0.10, 0.14±0.05 and 0.80±0.10 μm/min and 0.19±0.08, 0.13±0.04 and 0.83±0.09 μm/min, respectively. There was no significant difference in the elongation time and elongation rate of the spindle in all periods between the wild-type and *rok1*Δ strains (all P>0.05). These results indicate that the deletion of the *rok1* gene does not affect spindle dynamics at 25˚C.

The spindle elongation lengths at 37˚C showed that compared with the wild-type there was a significant decrease in the spindle elongation length of the *rok1*Δ strains at anaphase (10.38±1.02 vs. 9.33±0.83 μm, respectively); however, there were no significant changes in spindle elongation length at prophase or metaphase. Further analysis revealed that this trend was consistent for the spindle elongation time with wild-type strains displaying significantly longer elongation times compare with *rok1*Δ strains at anaphase (12.13±2.56 vs. 10.40±1.12 min, respectively), with no significant changes observed at prophase and metaphase (P>0.05) (Fig. 3E). In addition, there was no significant difference in spindle elongation rates between the wild-type and *rok1*Δ strains at prophase (0.26±0.06 vs. 0.23±0.05 μm/min, respectively), metaphase (0.10±0.06 vs. 0.08±0.05 μm/min, respectively) and anaphase (0.88±0.17 vs. 0.90±0.09 μm/min), respectively (both P>0.05) (Fig. 3F).

These results indicate that the *rok1* gene deletion decelerated the spindle elongation process at 37˚C. Comparison of 25˚C and 37˚C revealed that a high temperature stress of 37˚C had an inhibitory effect on the spindle elongation process.

Changes of actin during mitosis of rok1Δ strain under different temperature conditions. During mitosis, actin filaments co-assemble with myosin II to form an actomyosin

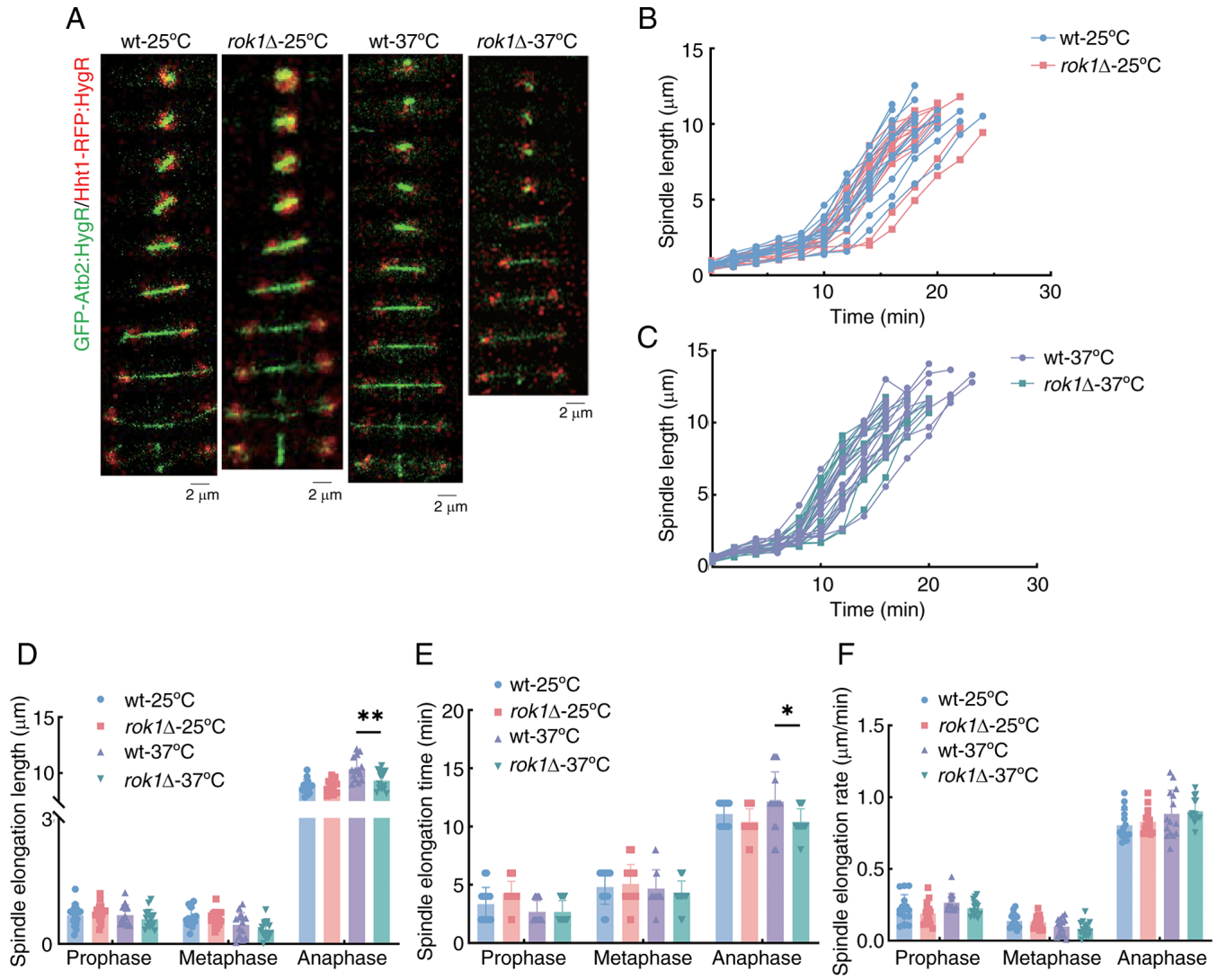

Figure 3. Effects of *rok1* deletion on spindle dynamics during mitosis in fission yeast. (A) Images of spindles during mitosis in wt and *rok1*Δ cells at 25˚C and 37˚. (B) Spindle length changes of wt and *rok1*Δ cells during mitosis at 25˚C. (C) Spindle length changes of wt and *rok1*Δ cells during mitosis at 37˚C. (D) Spindle elongation lengths of wt and *rok1*Δ cells at different phases. (E) Spindle elongation time of wt and *rok1*Δ cells at different phases. (F) Spindle elongation rates of wt and *rok1*Δ cells at different phases. *P<0.05 and **P<0.01; n=15. GFP, green fluorescent protein; RFP, red fluorescent protein; wt, wild-type.

ring that help the cell complete cytoplasmic division (42). Live-cell imaging was performed of wild-type and *rok1*Δ cells with Pact1-LifeAct-mGFP-tagged actin. Analysis of actin rings at 25˚C indicated that the actin ring length was significantly decreased (3.75±0.17 vs. 3.52±0.15 μm), total time from assembly to complete disappearance was significantly increased (28.70±2.84 vs. 31.40±1.29 min) and total contraction rates were significantly decreased (0.11±0.02 vs. 0.09±0.01 μm/min), in the *rok1*Δ strain compared with the wild-type stain (Fig. 4A-F). Further analysis results indicated that the assembly times of the actin rings in the wild-type and *rok1*Δ strains were 13.31±2.46 and 16.70±1.78 min, respectively, which was a significant difference (Fig. 4E). Entering the contraction phase, the actin rings of the wild-type and *rok1*Δ strains contracted for 15.39±0.85 and 14.70±1.92 min, respectively, and the contraction rates were 0.19±0.02 and 0.18±0.02 μm/min, respectively (Fig. 4F); there were no significant differences in contraction time and contraction rate (both P>0.05). These results indicate that *rok1* gene deletion prolongs the actin ring assembly process at 25˚C.

At 37˚C the contraction lengths were 4.09±0.38 vs. 3.50±0.26 μm and the total contraction rate of the actin ring was 0.12±0.02 vs. 0.09±0.01 μm/min for the wild-type and *rok1*Δ strains, respectively. Both actin ring length and total contraction rate were significantly decreased in the *rok1*Δ strain compared with the wild-type. However, the actin ring assembly time was 11.07±2.25 and 11.20±1.47 min for the wild-type and *rok1*Δ strains, respectively, which was not a significant difference (Fig. 4A-F). Entering the contraction phase, the contraction time and rate of the actin ring for the wild-type and *rok1*Δ strains were 15.60±3.22 vs. 15.33±1.95 min and 0.20±0.03 vs. 0.17±0.03 μm/min, respectively. The actin ring contraction rate of the *rok1*Δ strain was significantly decreased compared with the wild-type, and there was no significant difference in the contraction time (Fig. 4E and F). These results indicate that *rok1* gene deletion affected the contraction process of actin rings at 37˚C. Comparison of results at 25˚C and 37˚C revealed that *rok1* gene deletion both decreased the initiation length and contraction length of the actin ring and decreased the contraction

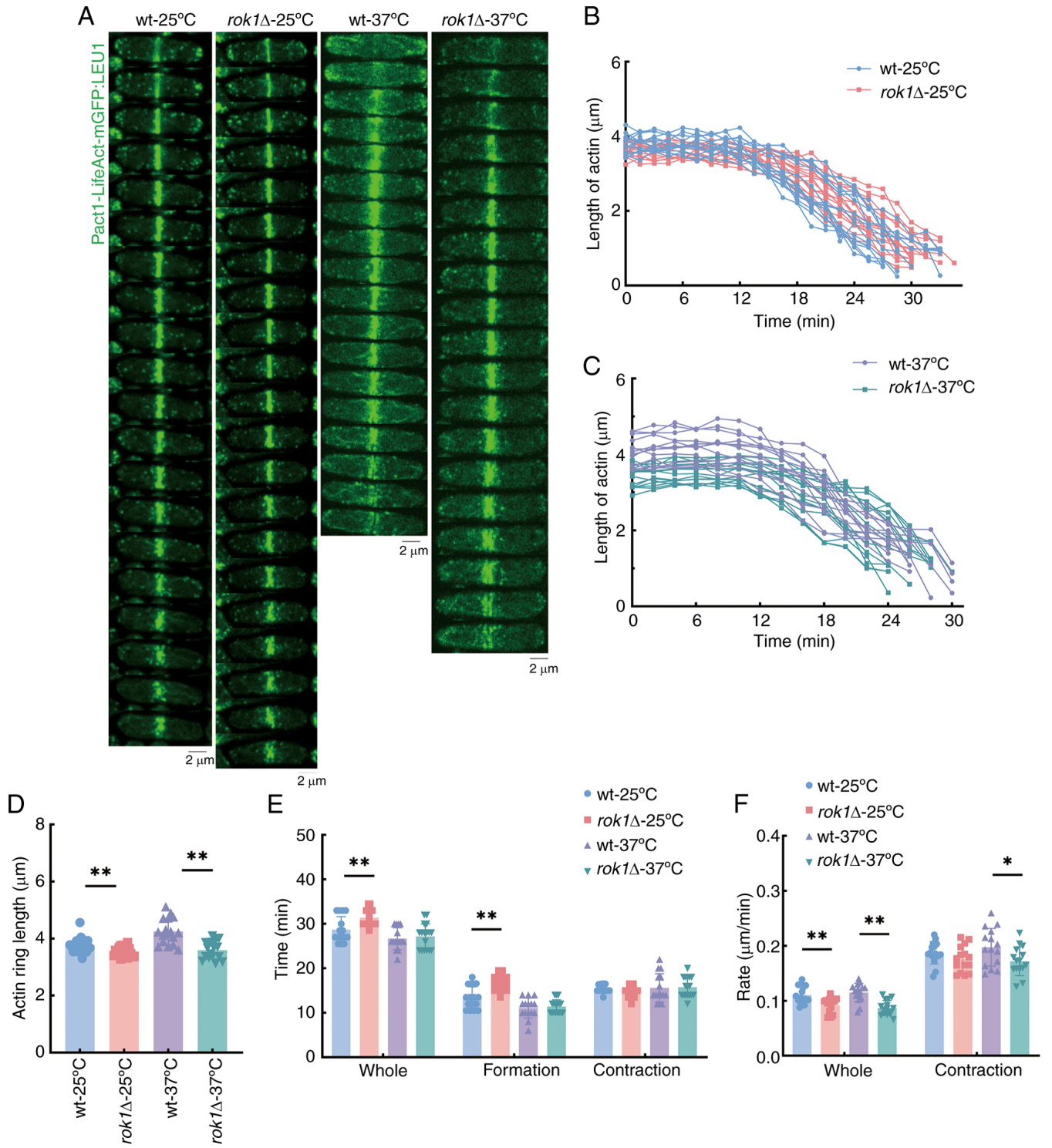

Figure 4. Effects of *rok1* deletion on actin dynamics during mitosis. (A) Images of the actin ring during mitosis in wt and *rok1*Δ cells at 25˚C and 37˚C. (B) Actin ring length changes of wild-type and *rok1*Δ cells during mitosis at 25˚C. (C) Actin ring length changes of wild-type and *rok1*Δ cells during mitosis at 37˚C. (D) The length of the actin ring of wild-type and *rok1*Δ cells. (E) The time of the actin ring formation and contraction of wild-type and *rok1*Δ cells at different phases. (F) The rate of the actin ring contraction of wild-type and *rok1*Δ cells at different phases. *P<0.05 and **P<0.01; n=15. GFP, green fluorescent protein; wt, wild-type.

rate. Unlike at 37˚C, *rok1* gene deletion prolonged the actin ring assembly process at 25˚C.

Changes of kinetochores during mitosis of rok1Δ strain at different temperature conditions. The kinetochores interact with spindle microtubules to assist in the correct segregation of chromosomes during mitosis. Live-cell imaging of wild-type and *rok1*Δ cells with Mis12-GFP-tagged kinetochore proteins. The analysis of kinetochore dynamics at 25˚C showed that the time from the separation to localization at the spindle poles of kinetochores in the wild-type and *rok1*Δ strains was 6.67±0.07 vs. 8.40±0.83 min, respectively, which was a significant

difference (Fig. 5A-D). Further analysis showed that the separation distance (9.44±0.78 vs. 10.06±0.67 μm) and separation time (11.87±1.60 vs. 13.87±2.07 min) were significantly increased in *rok1*Δ strains compared with wild-type, but there was no significant change in separation rates (0.81±0.11 vs. 0.74±0.10 μm/min) of kinetochores (Fig. 5E-G). These results indicate that *rok1* gene deletion prolonged the separation distance and separation time of kinetochores as well as the time for kinetochores to reach the poles of the spindle at 25˚C.

The time from the separation to localization at the spindle poles of kinetochores in the wild-type and *rok1*Δ strains was 5.60±1.12 and 6.63±0.92 min, respectively, at 37˚C, which was a significant difference (Fig. 5A-D). Further analysis indicated that the kinetochores separation distances of wild-type and *rok1*Δ strains were 10.08±0.78 and 10.45±0.08 μm, respectively, which was not significant difference (Fig. 5E). The separation time was significantly increased (11.60±1.12 vs. 13.73±2.12 min; Fig. 5F) and the rate of kinetochores was significantly decreased (0.88±0.09 vs. 0.78±0.13 μm/min; Fig. 5G) in *rok1*Δ strains compared with wild-type. These results indicate that *rok1* gene deletion delayed the kinetochore separation process at 37˚C. At 25˚C and 37˚C, *rok1* gene deletion prolonged the kinetochore segregation time, the time from the separation to localization at the spindle poles of kinetochores and thus delayed the kinetochore segregation process. The inhibition of the kinetochore segregation process was more effective with temperature stress at 37˚C.

Changes of centrosomes during mitosis of rok1Δ strain at different temperatures. During mitosis, centrosomes assist in the completion of microtubule assembly and influence the organization and function of the spindle. Live-cell imaging of wild-type and *rok1*Δ cells with Sid4-GFP-tagged centromere proteins was used to investigate changes in the centrosomes. The analysis of centrosome dynamics at 25˚C indicated that the total separation time was unchanged (19.87±0.52 vs. 19.87±1.92 min); however, the final separation distances (10.40±0.43 vs. 11.17±1.06 μm) and the total centrosome separation rates (0.52±0.03 vs. 0.56±0.02 μm/min) were significantly increased in *rok1*Δ strains compared with wild-type strains (Fig. 6A-F). Further analysis of the centrosome separation process revealed that the centrosome separation time of the wild-type and *rok1*Δ strains at the prophase were 6.00±1.07 and 5.07±1.28 min, at metaphase they were 4.13±0.52 and 4.40±1.12 min and at anaphase they were 9.73±1.03 and 10.40±1.35 min, respectively (Fig. 6E). The centrosome separation rates at prophase were 0.18±0.03 and 0.23±0.05 μm/min, at metaphase they were 0.11±0.06 and 0.16±0.08 μm/min and at anaphase the rates were 0.89±0.13 and 0.88±0.07 μm/min in the wild-type and *rok1*Δ strains, respectively. The centrosome separation time of *rok1*Δ strains at prophase was significantly decreased and the separation rate at prophase was significantly increased when compared with the wild-type. These results indicated that at 25˚C, *rok1* gene deletion resulted in increased centromere separation distance and increased separation rate.

When the experiments were conducted at 37˚C, the total separation time was not significantly altered (22.80±4.20 vs. 22.53±1.77 min); on the other hand, there was a significant decrease in both the final separation distance (12.90±1.44 vs. 10.82±0.63 μm) and the total centrosome separation rates (0.57±0.06 vs. 0.48±0.04 μm/min) in the *rok1*Δ strains compared with wild-type. Further analysis of the centrosome separation process revealed that the centrosome separation time of the wild-type and *rok1*Δ strains at different phases were as follows: Prophase, 4.53±1.41 and 7.07±2.12 min; metaphase, 4.80±1.82 and 3.87±1.60 min; and anaphase, 13.47±2.88 and 11.60±1.12 min, in wild-type and *rok1*Δ strains, respectively. The centrosome separation rates were as follows: Prophase, 0.23±0.06 and 0.16±0.05 μm/min; metaphase, 0.19±0.06 and 0.10±0.04 μm/min; and anaphase, 0.81±0.10 and 0.79±0.10 μm/min, in wild-type and *rok1*Δ strains, respectively. The centrosome separation time at prophase in the *rok1*Δ strain was significantly increased, but the separation time at anaphase was significantly decreased compared with the wild-type. Furthermore, the separation rate of the *rok1*Δ strain was significantly decreased at prophase and metaphase compared with the wild-type. These results indicated that at 37˚C, *rok1* gene deletion shortened the centrosome separation distance and decreased the separation rate. Comparison of results at 25 and 37˚C revealed that 37˚C high temperature stress reversed the effect of *rok1* gene deletion on the centrosome segregation process.

Sequencing quality analysis. Combining the three replicates, the total number of bases in the high-quality analyzed data for the wild-type-25˚C strain, the wild-type-37˚C strain, the *rok1*Δ-25˚C strain and the *rok1*Δ-37˚C strain were 6.80 Giga bases (G), 6.67 G, 6.88 G and 6.74 G, respectively. The $Q_{phred}20$ (percentage of bases with a phred score >20, where Phred=-10·log10(e) and e represents the sequencing error rate) (43) value of all four groups of samples was >98.00%, the $Q_{phred}30$ (percentage of bases with a Phred score >30) value was >94%, the GC content was between 41-43% and the sequencing error rate was <0.03%. These results suggest that the sequencing data were accurate and reliable and could be analyzed and studied subsequently.

Highly expressed gene analysis. Gene expression levels were quantitatively analyzed, with FPKM <1 as low or no gene expression, FPKM >1 as genes expressed, FPKM >60 as genes highly expressed and FPKM >5,000 as genes very highly expressed (35,44). The results indicated that there were 4,950, 7,757, 4,997 and 7,488 genes expressed in the wild-type-25˚C strain, the wild-type-37˚C strain, the *rok1*Δ-25˚C strain and the *rok1*Δ-37˚C strain, respectively, which accounted for 39.00, 61.11, 39.37 and 59.00% of the total genes capable of expression in fission yeast. In addition, there were 1,966, 2,181, 1,811 and 2,176 highly expressed genes, accounting for 15.17, 17.18, 14.27 and 17.14% of the total genes, respectively. From these highly expressed genes, representative genes exhibiting statistically significant expression differences between the *rok1*Δ strain and the wild-type strain were further selected for display (Fig. 7A and B; Tables III and IV).

Among the genes expressed to a very high level in both wild-type and *rok1*Δ-25˚C strains, the FPKM value of the *zym1* gene decreased by 1.629-fold compared to the wild-type strain (P<0.01). The FPKM values of the *tdh1* and *pgk1* genes increased by 1.1621- and 1.5047-fold, respectively

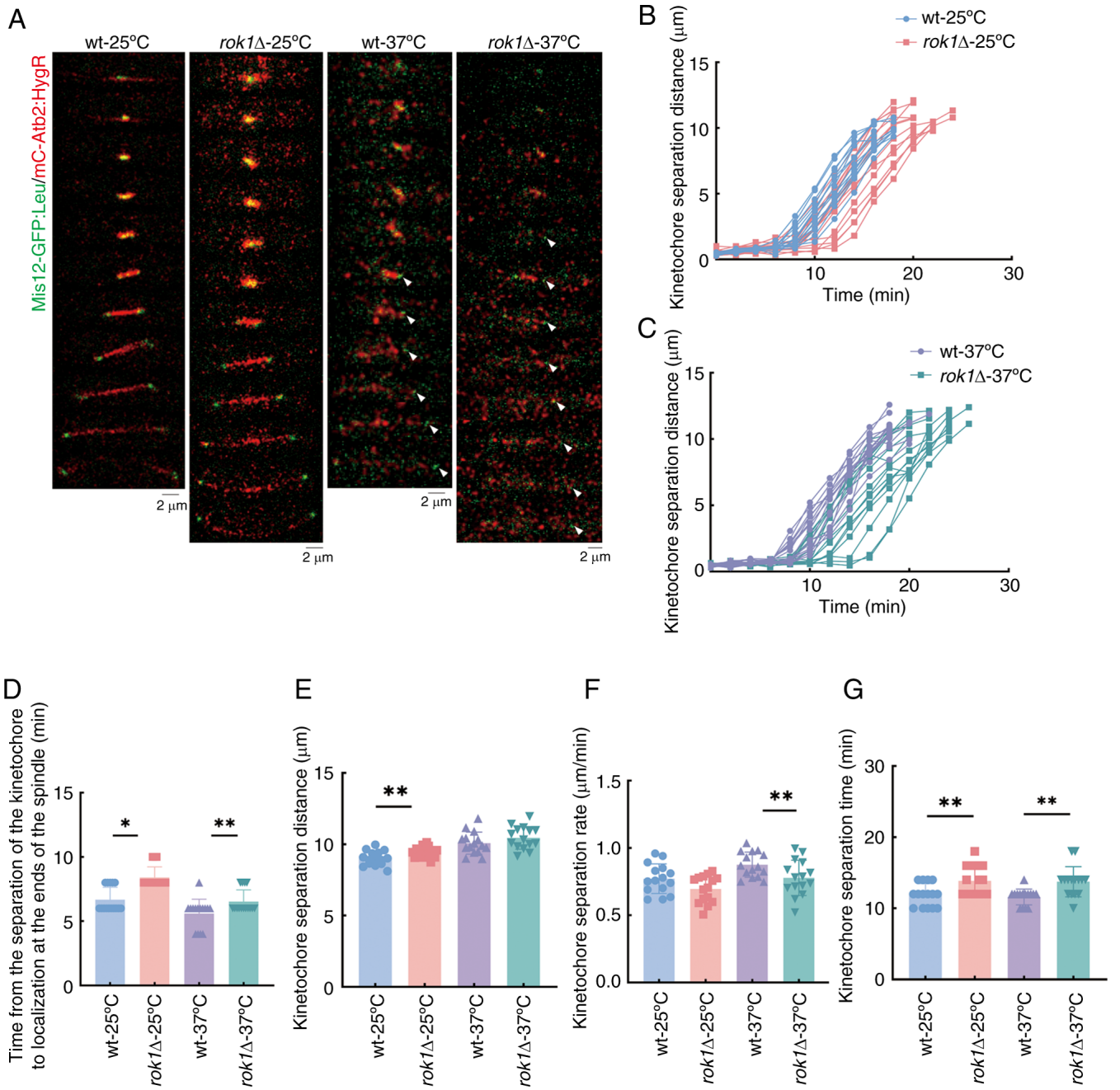

Figure 5. Effects of *rok1* deletion on kinetochore dynamics during mitosis in fission yeast. (A) Images of kinetochore during mitosis in wild-type and *rok1*Δ cells at 25˚C and 37˚C, white arrows indicated the position of kinetochores. (B) Kinetochore separation distance changes of wild-type and *rok1*Δ cells during mitosis at 25˚C. (C) Kinetochore separation distance changes of wild-type and *rok1*Δ cells during mitosis at 37˚C. (D) Time from the separation of the kinetochore to localize at the ends of the spindle in the wild-type and *rok1*Δ cells. (E) Kinetochore separation distance of wild-type and *rok1*Δ cells. (F) Kinetochore separation time of wild-type and *rok1*Δ cells. (G) Kinetochore separation rates of wild-type and *rok1*Δ cells. *P<0.05 and **P<0.01; n=15. GFP, green fluorescent protein; wt, wild-type.

(both P<0.01). Among the genes that were expressed at very high levels in both wild-type and *rok1Δ*-37˚C strains, the FPKM value of the *rpl3202* gene increased 1.6323-fold in the wild-type strain (P<0.05). The FPKM values of *trx1* and *plr1* genes were decreased by 0.4418-fold (P<0.05) and 0.5132-fold (P<0.01), respectively.

Analysis of differentially expressed genes. The differentially expressed genes of the wild-type strain and the *rok1*Δ-25˚C and *rok1*Δ-37˚C strains were analyzed. The results indicated that there were 3,034 and 1,695 differentially expressed genes in the *rok1*Δ-25˚C and *rok1*Δ-37˚C strains, respectively, compared with the wild-type strains, which included 1,482 and 705 upregulated genes and 1,552 and 990 downregulated genes, respectively (Fig. 7C and D).

Compared with the wild-type strain, in the *rok1*Δ-25˚C strain, *mei2*, *map2*, *map3* and *psc3* gene expression were upregulated by 1.2866-, 1.8764-, 2.7593- and 1.3973-fold, respectively (Table V). In the *rok1*Δ-37˚C strain, *gpa2*, *rgs1*, *myo51* and *blt1* gene expression was upregulated by 1.9694-, 2.1606-, 0.7366- and 1.0046-fold, respectively (Table VI). In the *rok1*Δ-25˚C strain, *ddx27* and *pas1* gene expression were downregulated

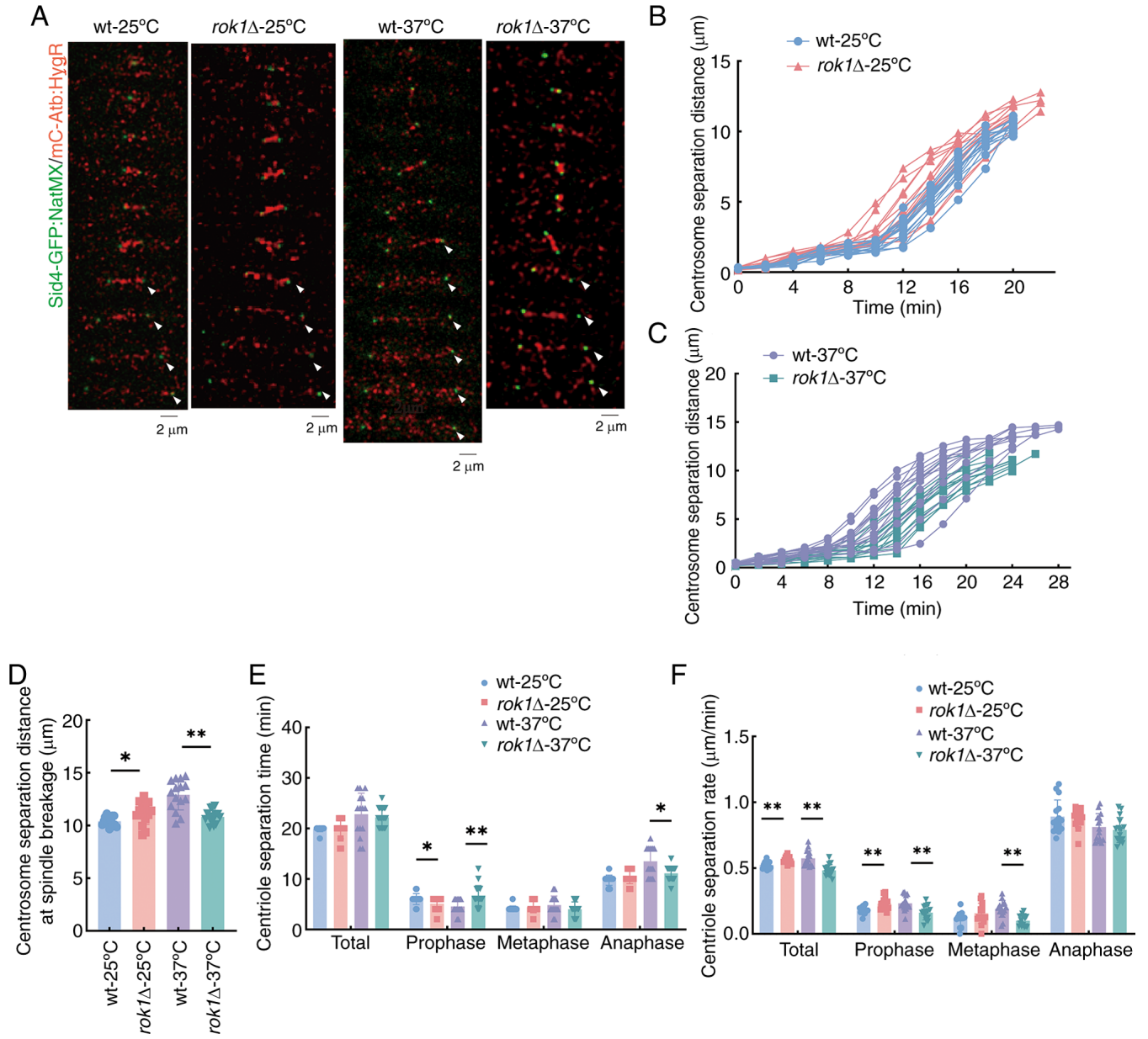

Figure 6. Effects of *rok1* deletion on centrosome dynamics during mitosis in fission yeast. (A) Images of centrosome during mitosis in wt and *rok1*Δ cells at 25˚C and 37˚C, white arrows indicated the position of centrosome. (B) Centrosome separation distance changes of wt and *rok1*Δ cells during mitosis at 25˚C. (C) Centrosome separation distance changes of wt and *rok1*Δ cells during mitosis at 37˚C. (D) Centrosome separation distance in the wt and *rok1*Δ cells at spindle breakage. (E) Centrosome separation time of wt and *rok1*Δ cells at different phases. (F) Centrosome separation rates of wt and *rok1*Δ cells at different phases. *P<0.05 and **P<0.01; n=15. GFP, green fluorescent protein; wt, wild-type.

by 1.7320- and 1.6148-fold, respectively (Table VII). In the *rok1*Δ-37˚C strain, *rho5*, *wos2*, *apc14*, and *pas1* genes were downregulated by 1.4299-fold, 1.1209-fold, 0.7467-fold, and 1.3259-fold, respectively. *arp1*, *dil1*, *cmk1* and *mfr1* gene expression were downregulated by 0.9087-, 1.6737-, 1.3417- and 1.1414-fold, respectively (Table VIII). Notably, although *arp1*, *dli1*, *cmk1*, and *mfr1* genes were all significantly downregulated, the downregulation factor for *arp1* was 0.9087-fold, lower than that of the other genes (>1). This result indicates that while the deletion of the *rok1* gene broadly suppresses the transcription of these genes, its inhibitory effect on arp1 is relatively weaker.

Differential gene expression validation. Analysis of differentially expressed genes from the transcriptomic data revealed that *psc3* and *psm1* were key genes at 25˚C, whereas *myo51* and *blt1* were key genes at 37˚C. To validate the expression changes of these genes, specific primers were designed using *act1* as the reference gene and verified for specificity through the NCBI Primer-BLAST tool. The results demonstrated that in the *S. pombe* (taxid: 4896) genome, the primers for *psc3*, *psm1*, *myo51*, *blt1* and *act1* all specifically matched unique target sequences, confirming the validity of the primer design and their suitability for RT-qPCR experiments.

The RT-qPCR results showed that the expression levels of *psc3* and *psm1* were significantly upregulated at 25˚C (Fig. 8A); in addition, *myo51* and *blt1* were significantly upregulated at 37˚C (Fig. 8B) with *rok1* deletion compared with the wild-type. These findings were consistent with the

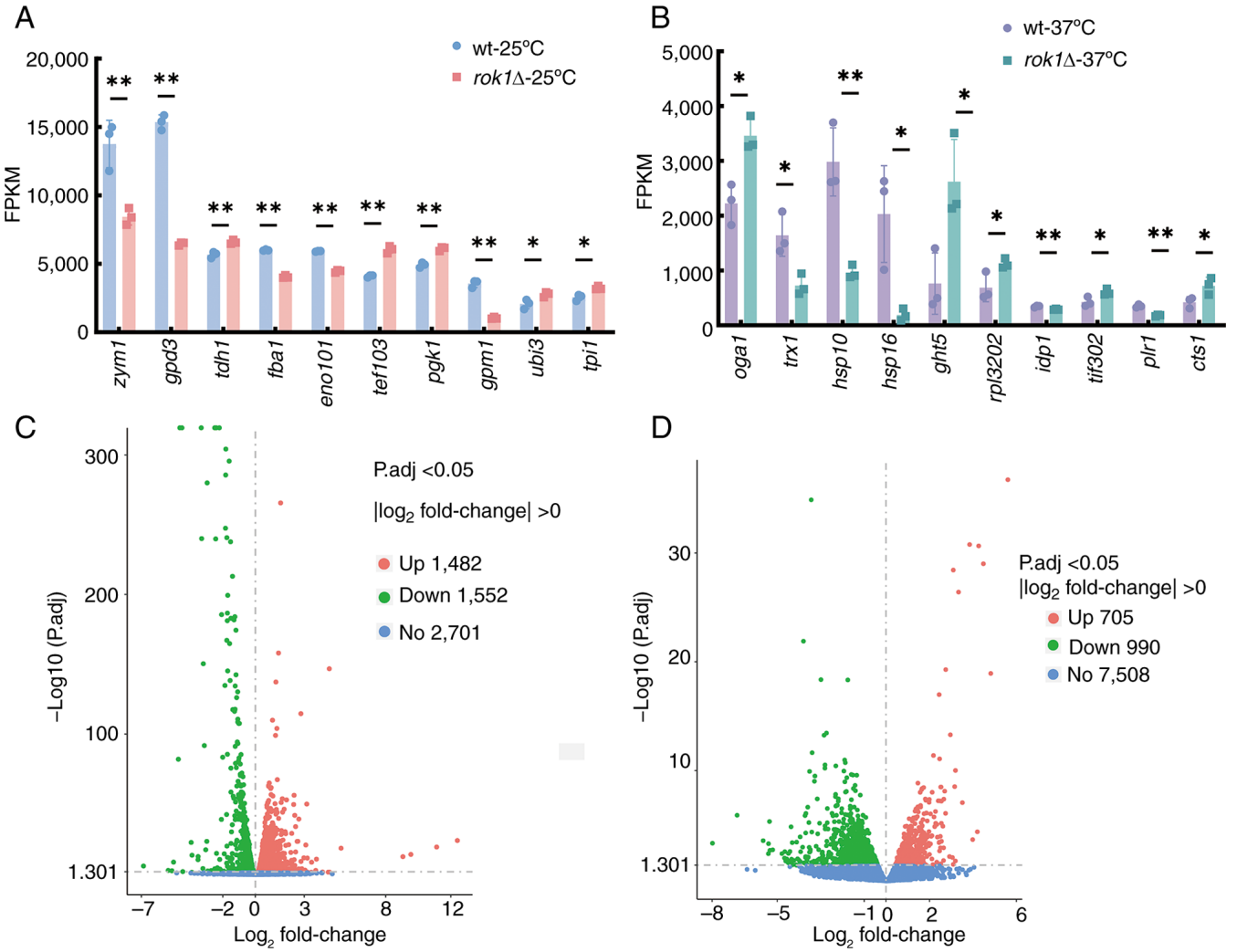

Figure 7. Analysis of highly expressed genes and differentially expressed genes. (A) Differential analysis of highly expressed genes in the wt and *rok1*Δ strains at 25˚C. (B) Differential analysis of highly expressed genes in the wt and *rok1*Δ strains at 37˚C. (C) Volcano plot of differently expressed genes in the wt and *rok1*Δ strains at 25˚C. (D) Volcano plot of differently expressed genes in the wt and *rok1*Δ strains at 37˚C. *P<0.05 and **P<0.01. n=3. FPKM, fragments per kilobase million; wt, wild-type.

RNA-Seq data, confirming the reliability of the transcriptomic results. These results suggest that *rok1* regulate the expression of these key genes, thereby influencing the dynamics of mitotic progression.

Differential gene GO functional enrichment analysis. GO enrichment analysis of differentially expressed genes was performed in wild-type and *rok1*Δ strains, and the 10 categories with the most significant up- and downregulated differentially expressed genes were selected and plotted as bar graphs. The analysis revealed that at 25˚C, the *rok1*Δ strain was enriched for differential genes up to 303 GO branches (P≤0.05), including 230 biological processes, 41 cellular components and 32 molecular functions, compared with the wild-type strain. Among the biological processes, upregulated genes were enriched in 'sister chromatid segregation' and 'reproductive process'. In cellular components, upregulated genes were enriched in 'chromosomes, centromeric region' and 'condensed chromosome inner kinetochore' regions. In molecular function, upregulated genes were enriched in 'nucleoside-triphosphatase activity' and 'translation elongation factor activity' (Fig. 9A). In addition, downregulated differential genes were enriched in 'purine-containing compound metabolic process' and 'actin cortical patch organization', 'actin cortical patch' and 'plasma membrane' regions in cellular components, with 'transmembrane transporter activity' and 'oxidoreductase activities' in molecular functions (Fig. 9B).

At 37˚C, the differential genes of the *rok1*Δ strain were enriched in 28 GO branches (P≤0.05), including 3 biological processes and 25 cellular components. compared with the wild-type strain. upregulated genes were enriched in 'transmembrane transport' and 'ribosome biogenesis' during biological processes; in cellular components, upregulated genes were enriched in the 'ribosome'; in molecular function, upregulated genes were enriched in 'transmembrane transporter activity' and 'RNA polymerase II transcription factor activity, sequence-specific DNA binding' (Fig. 10A). In addition, downregulated differential genes were enriched in 'protein folding 'and 'actin filament-based' processes, 'mitochondrial outer membrane' and 'proteasome core complex' regions in cellular components and 'hydrolase activity, acting

Table III. Highly expressed genes in the wt-25˚C and *rok1*Δ-25˚C strains.

Gene	FPKM (wt)	FPKM (*rok1*Δ)	Description
zym1	13,760.91	8,448.89	Metallothionein, Zym1
gpd3	15,353.45	6,483.99	Glyceraldehyde 3-phosphate dehydrogenase, Gpd3
tdh1	5,679.17	6,599.78	Glyceraldehyde-3-phosphate dehydrogenase, Tdh1
fba1	6,012.45	4,059.26	Fructose-bisphosphate aldolase, Fba1
eno101	5,927.17	4,461.72	Enolase
tef103	4,107.47	6,054.25	Translation elongation factor EF-1 α, Ef1a-c
pgk1	4,919.32	6,107.86	Phosphoglycerate kinase, Pgk1
gpm1	3,555.49	1,041.72	BPG-dependent phosphoglycerate mutase (PGAM), Gpm1
ubi3	2,068.30	2,770.01	Ribosomal-ubiquitin fusion protein, Ubi3
tpi1	2,552.69	3,237.18	Triosephosphate isomerase

FPKM, fragments per kilobase million; wt, wild-type.

Table IV. Highly expressed genes in the wt-37˚C and *rok1*Δ-37˚C strains.

Gene	FPKM (wt)	FPKM (*rok1*Δ)	Description
oga1	2,229.10	3,462.16	Ribosome preservation factor, Stm1 homolog, Oga1
trx1	1,644.48	726.54	Cytosolic thioredoxin, Trx1
hsp10	2,983.73	964.69	Mitochondrial heat shock protein, Hsp10
hsp16	2,031.58	187.98	Heat shock protein, Hsp16
ght5	762.67	2,620.96	Plasma membrane high-affinity proton symporter, Ght5
rpl3202	687.85	1,122.77	60S ribosomal protein L32
idp1	346.51	292.29	Isocitrate dehydrogenase, Idp1
tif302	427.34	604.58	Translation initiation factor eIF3b (p84)
plr1	351.44	180.39	Pyridoxal reductase, Plr1
cts1	424.50	722.51	CTP synthase, Cts1

FPKM, fragments per kilobase million; wt, wild-type.

on glycosyl bonds' in molecular functions (Fig. 10B). The GO enrichment results indicate that the ribosome biogenesis process of the *rok1*Δ strain was affected, the mitotic cytoskeleton was abnormal and the normal cell growth and reproduction process was disrupted.

Differential gene KEGG enrichment analysis. KEGG enrichment analysis was performed on the differentially expressed genes of the wild-type strain and the *rok1*Δ strain, and the top 10 pathways of selected upregulated genes and downregulated genes were plotted as bar graphs (Fig. 11A and B). The results indicated that 1,634 differential genes were enriched in 80 pathways in the *rok1*Δ-25˚C strain. The upregulated genes were enriched in pathways such as 'ribosome', 'cell cycle-yeast' and 'proteasome', whereas the downregulated genes were enriched in pathways such as 'MAPK signaling pathway-yeast' and 'citrate cycle (TCA cycle)'. The *rok1*Δ-37˚C strain was enriched for 787 differential genes in 89 pathways. Upregulated genes were enriched in pathways such as 'ribosome', 'ribosome biogenesis in eukaryotes' and 'DNA replication', whereas downregulated genes were mainly enriched in pathways such as 'autophagy-yeast' and 'protein processing in endoplasmic reticulum'. At 25˚C, the 'cell cycle-yeast' pathway was enriched for 27 upregulated genes (Fig. 11A). The genes that were upregulated in this pathway included *spo4*, *rad17*, *psm1*, *mis4* and *mad1*. At 37˚C, the 'autophagy-yeast' pathway was enriched for 18 downregulated genes (Fig. 11B). The major genes with downregulated expression in this pathway included *pas1*, *atg17*, *atg13*, *atg15* and *arc1*.

Discussion

In transcriptomic analysis, highly expressed genes indicate the core functions and active metabolic pathways of cells under specific conditions, serving as a crucial entry point and a central analytical step for uncovering cellular functions and adaptive mechanisms. Among the genes expressed to a very high level in both wild-type and *rok1*Δ-25˚C strains was

Table V. Upregulated differentially expressed genes in the wild-type-25˚C and *rok1*Δ-25˚C strains.

Gene	log_2FoldChange	Adjusted P-value	Length, bp	Description
hsp90	1.5155	$3.25x10^{-266}$	2,600	Hsp90 chaperone
ght2	1.2251	$6.59x10^{-138}$	2,245	Hexose transmembrane transporter, Ght2
map3	2.7593	$3.18x10^{-115}$	2,888	Pheromone M-factor receptor, Map3
bip1	1.0174	$1.60x10^{-110}$	2,805	ER heat shock protein, BiP
mei2	1.2866	$1.24x10^{-104}$	4,033	RNA-binding protein involved in meiosis, Mei2
map2	1.8764	$1.91x10^{-53}$	3,726	P-factor pheromone Map2
tef101	0.7861	$5.12x10^{-53}$	1,569	Translation elongation factor EF-1 α, Ef1a-a
wtf25	1.5509	$1.45x10^{-51}$	2,271	Wtf element
psc3	1.3973	$3.73x10^{-40}$	3,989	Mitotic cohesin complex, non-SMC subunit, Psc3
ctt1	0.6184	$1.83x10^{-39}$	2,212	Catalase

bp, base pair; ER, endoplasmic reticulum.

Table VI. Upregulated differentially expressed genes in the wild-type-37˚C and *rok1*Δ-37˚C strains.

Gene	log_2FoldChange	Adjusted P-value	Length, bp	Description
ppk1	2.4226	$6.88x10^{-15}$	3,072	Serine/threonine protein kinase, Ppk1
rgs1	2.1606	$1.98x10^{-9}$	1,446	Regulator of G-protein signaling, Rgs1
put4	3.1716	$3.38x10^{-8}$	1,659	Plasma membrane proline transmembrane transporter, Put4
snoR54b	2.5113	$7.20x10^{-7}$	96	Small nucleolar RNA, snR54b
uck2	1.6349	$9.23x10^{-7}$	663	Uracil phosphoribosyltransferase, Uck2
gpa2	1.9694	$6.84x10^{-6}$	1,065	Heterotrimeric G protein α-2 subunit, Gpa2
myo51	0.7366	$1.52x10^{-2}$	4,416	Myosin type V
fib1	0.7617	$1.74x10^{-2}$	918	Fibrillarin, rRNA and histone methyltransferase
blt1	1.0046	$3.53x10^{-2}$	2,103	Ubiquitin domain-like protein, Blt1
tif11	0.6131	$3.54x10^{-2}$	417	Translation initiation factor eIF1A

bp, base pair; rRNA, ribosomal RNA.

Table VII. Downregulated differentially expressed genes in the wild-type-25˚C and *rok1*Δ-25˚C strain.

Gene	log_2FoldChange	Adjusted P-value	Length, bp	Description
bgl2	-1.8472	$7.99x10^{-305}$	1,654	Glucan β-glucosidase, Bgl2
mae2	-1.6447	$3.56x10^{-296}$	2,080	Malic enzyme, malate dehydrogenase, Mae2
ddx27	-1.7320	$5.34x10^{-200}$	2,423	ATP-dependent RNA helicase, Ddx27/Drs1
prz1	-1.7525	$2.89x10^{-187}$	3,442	Calcineurin responsive transcription factor, Prz1
gal7	-2.1082	$3.39x10^{-186}$	1,566	Galactose-1-phosphate uridylyltransferase, Gal7
pas1	-1.6148	$1.99x10^{-165}$	3,109	Cyclin, Pas1
sgf73	-3.2303	$5.61x10^{-151}$	1,416	SAGA complex subunit, Sgf73
per1	-1.5861	$5.54x10^{-139}$	2,963	Plasma membrane amino acid permease, Per1
shd1	-0.7636	$1.83x10^{-47}$	4,782	Cytoskeletal protein binding protein Sla1 family, Shd1
mbx1	-1.2067	$1.88x10^{-45}$	3,183	MADS-box transcription factor, Mbx1

bp, base pair.

Table VIII. Downregulated differentially expressed genes in the wild-type-37˚C and *rok1*Δ-37˚C strain.

Gene	log_2FoldChange	Adjusted P-value	Length, bp	Description
rho5	-1.4299	$1.39x10^{-6}$	603	Rho family GTPase, Rho5
mbx1	-1.8473	$1.56x10^{-6}$	1,374	DNA-binding transcription factor, MADS-box, Mbx1
adg1	-1.8871	$1.73x10^{-6}$	501	*Schizosaccharomyces pombe* specific protein, Adg1
vip1	-1.2490	$1.50x10^{-3}$	774	RNA-binding protein, Vip1
wos2	-1.1209	$1.54x10^{-3}$	561	p23 homolog, Hsp90 co-chaperone, Wos2
mug125	-1.0961	$1.56x10^{-3}$	858	*Schizosaccharomyces pombe* specific protein, Mug125
pas1	-1.3259	$9.58x10^{-3}$	1,236	Cyclin, Pas1
apc14	-0.7467	$3.10x10^{-2}$	324	Anaphase-promoting complex subunit, Apc14
arp1	-0.9087	$3.44x10^{-2}$	1,140	Dynactin complex subunit, centractin family actin-like protein, Arp1
dli1	-1.6737	$4.40x10^{-2}$	1,083	Meiotic dynein intermediate light chain, Dli1
cmk1	-1.3417	$4.60x10^{-5}$	1,008	Calcium/calmodulin-dependent protein kinase, Cmk1
mfr1	-1.1414	$8.59x1^{0-4}$	1,266	Meiotic APC activator, Mfr1

bp, base pair.

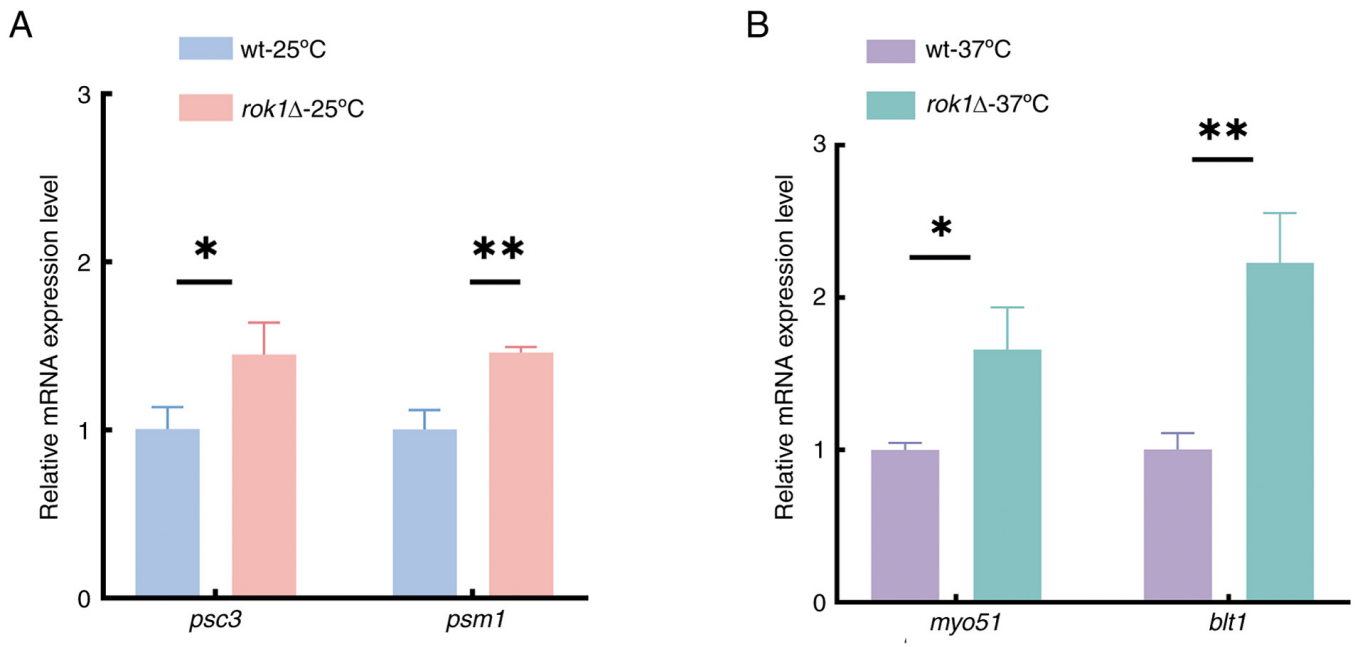

Figure 8. RT-qPCR verification of key differentially expressed genes. (A) Relative mRNA expression of *psc3* and *psm1* determined by RT-qPCR at 25˚C. (B) Relative mRNA expression of *myo51* and *blt1* determined by RT-qPCR at 37˚C. *P<0.05 and **P<0.01. RT-qPCR, reverse transcription quantitative PCR; wt, wild-type.

the *zym1* gene. This encodes the metallothionein Zym1, and deletion of the *zym1* gene results in aberrant segregation of meiotic chromosomes and aberrant spore formation (14,23). The FPKM values of *zym1* were decreased in the *rok1*Δ-25˚C strain, which is in agreement with the spore production anomaly in the present study. The *tdh1* gene encodes the glyceraldehyde-3-phosphate dehydrogenase Tdh1, which physically binds to the response regulator Mcs4 and the stress-responsive MAPKKK and is involved in the positive regulation of the MAPK cascade response. Through phosphorylation, the MAPK pathway delivers model factors that regulate biological growth and division-related signaling (45). The *pgk1* gene encodes the phosphoglycerate kinase Pgk1, which can be phosphorylated by the cell cycle protein-dependent kinase CDK1, and thus participates in cellular glycolysis as well as gluconeogenesis, providing energy for cell division, growth, and protein synthesis (46). FPKM values of *tdh1* and *pgk1* were upregulated in the *rok1*Δ-25˚C strain, which suggested that phosphorylation of the MAPK signaling pathway and glycolytic processes was being compensated.

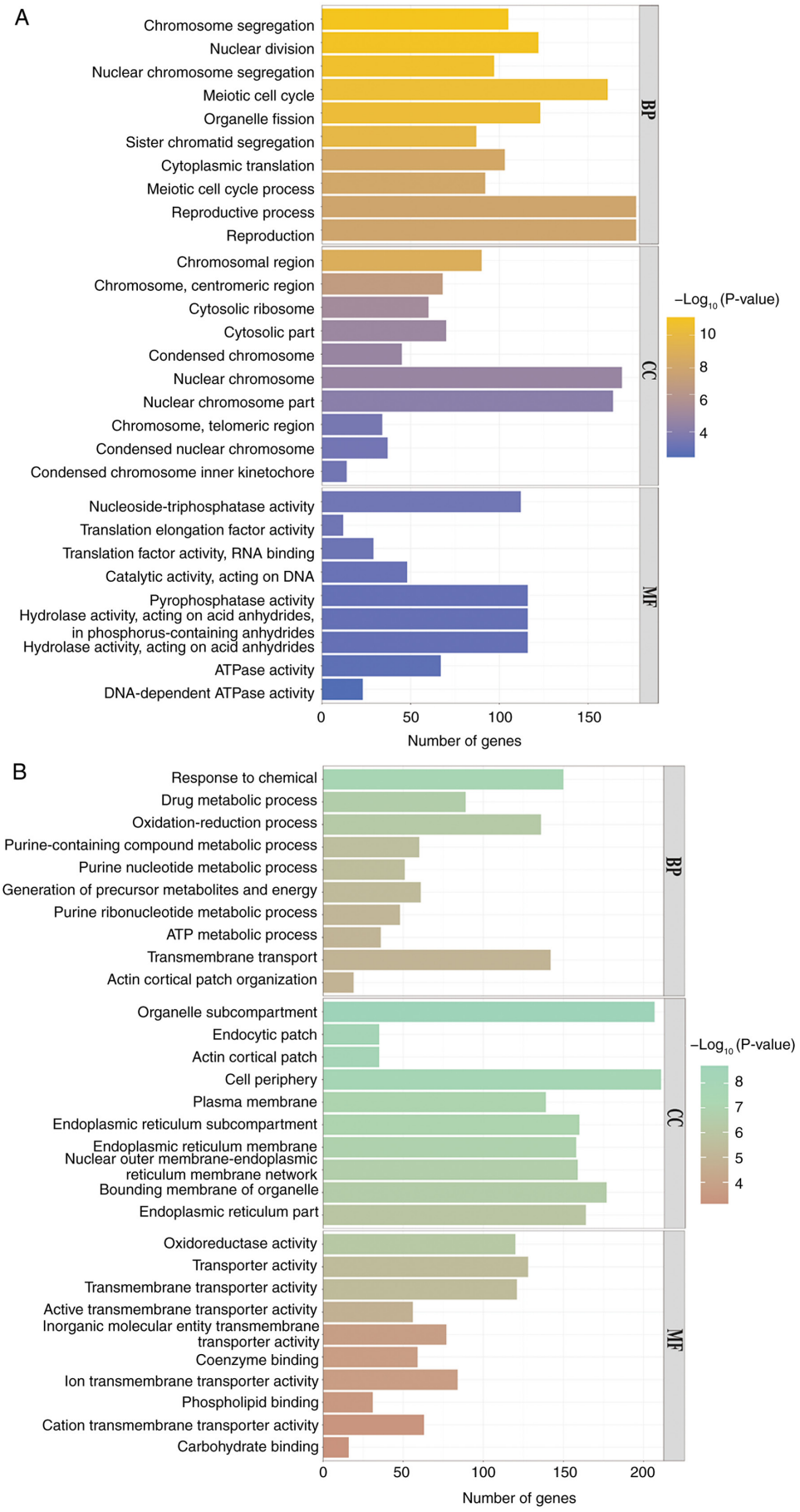

Figure 9. GO enrichment results of differentially expressed genes in the wild-type and *rok1*Δ strains at 25˚C. (A) GO enrichment results for upregulated differential genes at 25˚C. (B) GO enrichment results for downregulated differential genes at 25˚C. GO, Gene Ontology; BP, biological process; CC, cellular component; MF, molecular function.

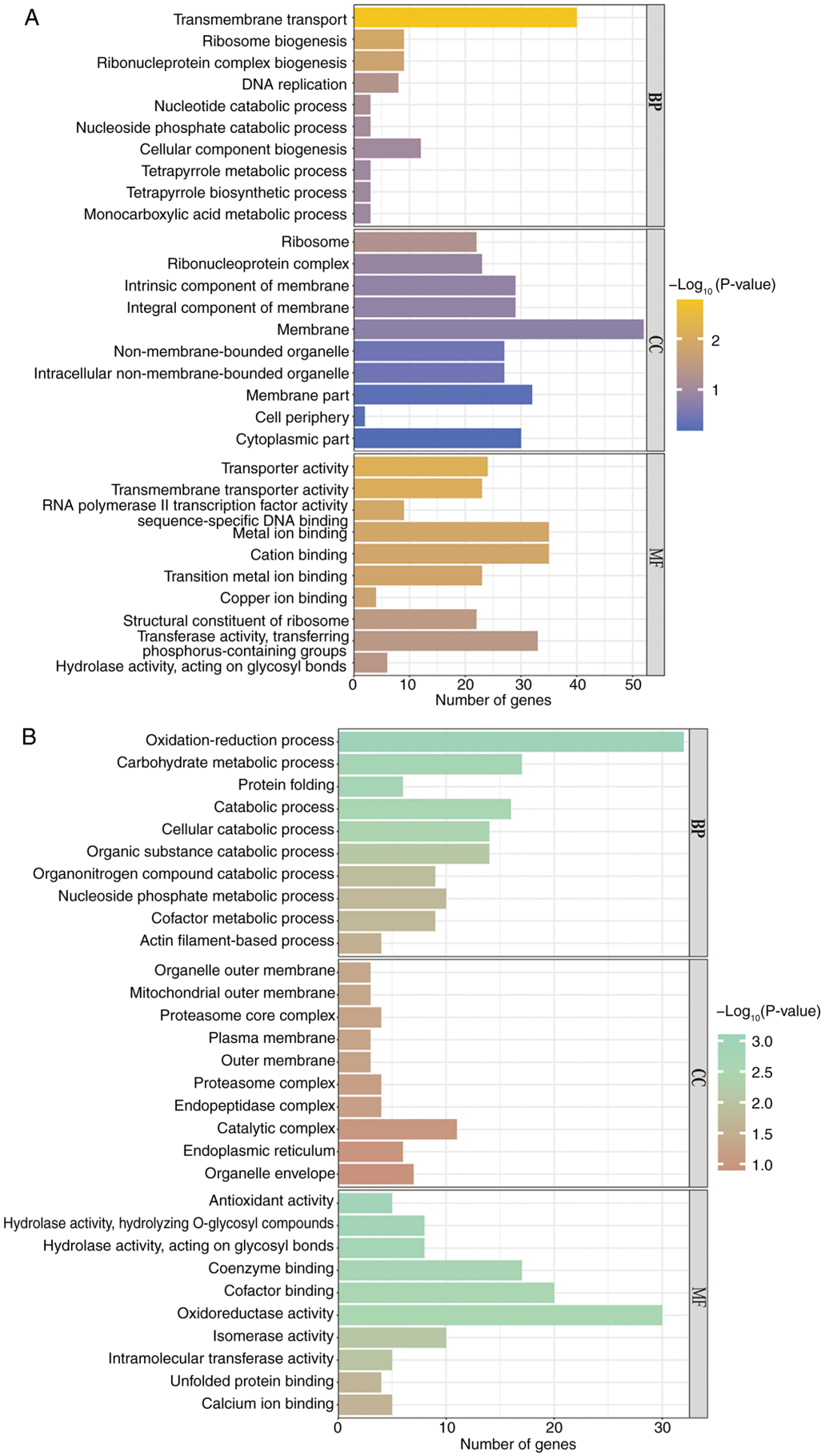

Figure 10. GO enrichment results of differentially expressed genes in the wild-type and *rok1*Δ strains at 37˚C. (A) GO enrichment results for upregulated differential genes at 37˚C. (B) GO enrichment results for downregulated differential genes at 37˚C. GO, Gene Ontology; BP, biological process; CC, cellular component; MF, molecular function.

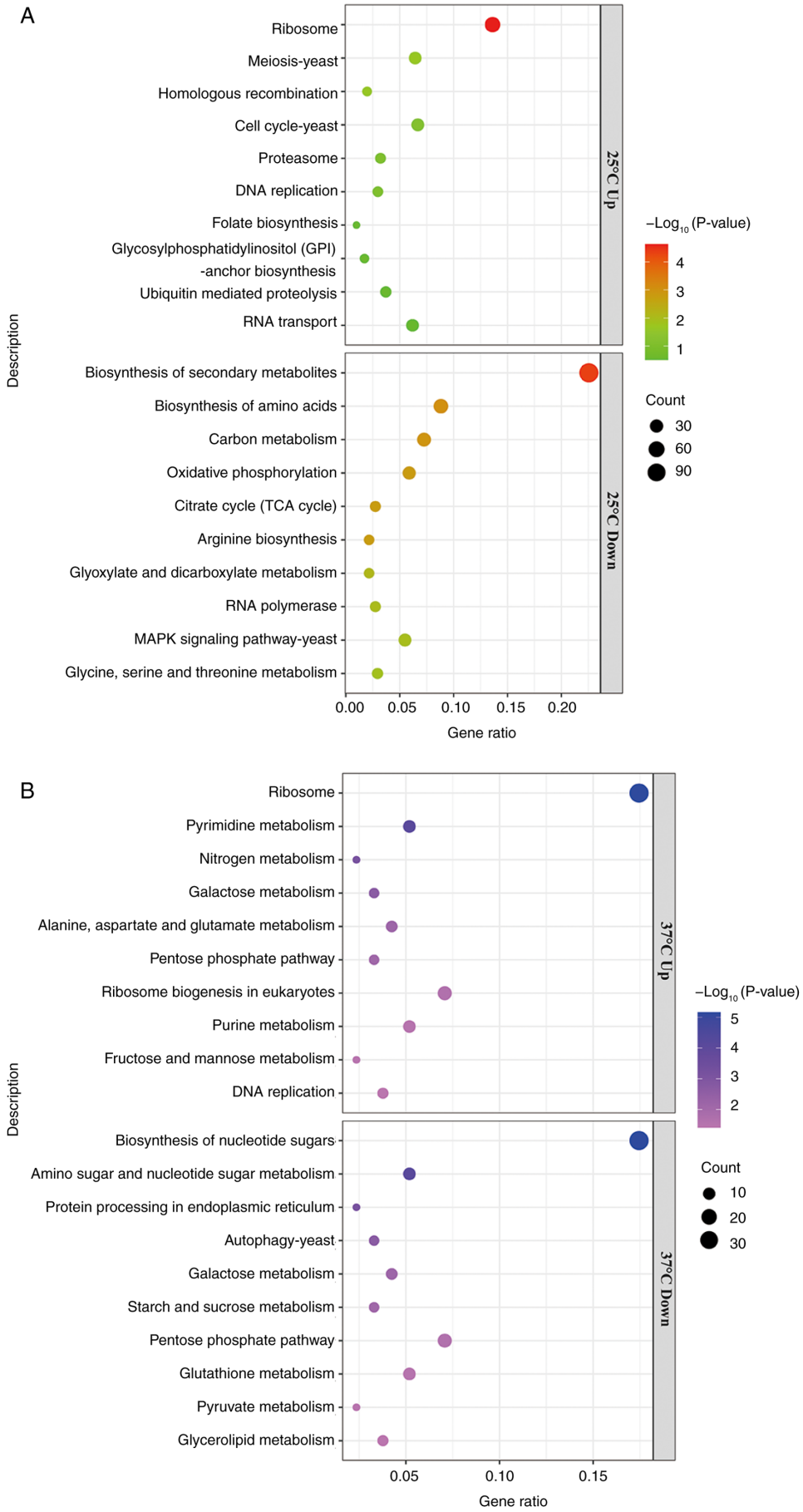

Figure 11. KEGG enrichment results of differentially expressed genes in the wild-type and *rok1*Δ strains. (A) KEGG enrichment results for upregulated and downregulated differential genes at 25˚C. (B) KEGG enrichment results for upregulated and downregulated differential genes at 37˚C. KEGG, Kyoto Encyclopedia of Genes and Genomes.

Among the genes that were expressed at very high levels in both wild-type and *rok1*Δ-37˚C strains was the *trx1* gene, which encodes the cytosolic thioredoxin Trx1, whose deletion results in abnormal DNA replication checkpoints in mitosis and spore formation (23,47). The *plr1* gene encodes the pyridoxal reductase Plr1, which is involved in the process of pyridoxal biosynthesis, whereas *plr1* gene deletion results in abnormal sporulation (23). The FPKM values of *trx1* and *plr1* were downregulated in the *rok1*Δ-37˚C strain, which indicated abnormal cell cycle progression and sporulation, which was consistent with the abnormalities of cell division in the *rok1*Δ-37˚C strain. The *rpl3202* gene encodes the 60S ribosomal protein L32, which participates in ribosome composition and cytoplasmic translation processes as a cytosolic large ribosomal subunit component and directs mitotic protein synthesis (48). The FPKM value of *rpl3202* was increased in the *rok1*Δ-37˚C strain, which suggested that ribosome composition and translation processes had been compensated.

Differential gene analysis can directly reveal the molecular mechanisms, key regulatory pathways, and potential functional targets underlying phenotypic differences by deciphering the dynamic changes in gene expression under different conditions (49). In this study, we conducted further analysis of differentially expressed genes between the wild-type and *rok1*Δ strains. The results showed that among the genes upregulated in the *rok1*Δ-25˚C strain, the *mei2* gene encodes the RNA-binding protein involved in meiosis Mei2, which switches the cell from a mitotic cell cycle to a meiotic cell cycle by dephosphorylation, allowing the cell to stably express meiosis-specific mRNAs (50). The *map2* gene encodes the P-factor pheromone Map2 and *map3* encodes the pheromone M-factor receptor Map3. Both Map2 and Map3 are involved in the pheromone-responsive MAPK cascade; map2 is involved in the positive regulation of cell fusion coupling through signaling (51-53). The *psc3* gene encodes the STAG protein subunit Psc3 of the mitotic cohesin complex, which assembles with Rad21, Psm1 and Psm3 into a functional complex. This complex maintains the connection between sister chromatids through physical interactions, participates in establishing and sustaining sister chromatid cohesion, and ensures accurate chromosome segregation (54). The *psc3* gene is consistent with the lagging of centromeres observed in this study at 25˚C, suggesting that the Rok1 protein participates in regulating the formation and maintenance of cohesion between sister chromatids.

Among the genes upregulated in the *rok1*Δ-37˚C strain (Table VI), the *gpa2* gene encodes a protein that is a structural component of the mitotic spindle pole body, and Gpa2 is involved in the regulation of mitotic progression (55). The *rgs1* gene encodes the regulator of G-protein signaling Rgs1, and *rgs1* gene deletion affects the pheromone-responsive MAPK cascade response process and results in aberrant protein localization in the actin fusion focus (56). The *myo51* gene encodes a type V myosin whose motor domain and tail domain interact with actin filaments, effectively mediating the integration of nodes into the actin filament network, thereby regulating the actin ring assembly and cytokinesis (57-59). Myo51 can participate in CAR assembly and cytokinesis process together with myosin II. Studies have shown that at 29˚C, cells lacking myo51 can maintain normal morphology and growth rate, whereas overexpression of myo51 leads to elongated cells and failure to form functional septa, exhibiting phenotypes similar to those observed in the present study; this indicates that Myo51 plays a non-essential role in cytokinesis (60). Further research has revealed that Myo51 primarily plays a critical role in the assembly phase of the contractile ring but cannot independently drive ring contraction during the constriction phase (61). The present findings demonstrate a slowed contraction rate of the actin ring, accompanied by upregulated expression of myo51 according to transcriptomic data; however, the specific molecular mechanisms underlying this phenomenon require further investigation. The *blt1* gene encodes the ubiquitin domain-like protein Blt1, which possesses cytoskeletal protein-membrane anchoring activity. It recruits the Nod1-Gef2 complex to form a cell division node, assembles the mitotic actomyosin contractile ring, and participates in cytokinesis (62,63). In summary, the upregulation of *myo51* and *blt1* may be a key factor underlying the impaired actin ring assembly observed in the *rok1*Δ strain at 37˚C in this study. These findings suggest that the Rok1 protein may influence actin polymerization, thereby participating in the regulation of actin ring assembly, contraction, and cytokinesis.

Among the genes downregulated in the *rok1*Δ-25˚C strain, the *ddx27* gene encodes the ATP-dependent RNA helicase Ddx27/Drs1, which regulates rRNA processing during ribosome biogenesis, and deletion of the *ddx27* gene results in abnormal mitotic cell cycle (15). The *pas1* gene encodes the cyclin Pas1, which as a partner protein of the cell cycle protein-dependent protein kinase Pho85/PhoA-like Pef1, is involved in the negative regulation of sister chromatid cohesion together with Pef1 (64). The downregulation of the *pas1* gene correlates with the observed lagging of centromeres at 25˚C in this study, suggesting that the Rok1 protein participates in regulating the formation and maintenance of cohesion between sister chromatids.

Among the genes downregulated in the *rok1*Δ-37˚C strain, the *rho5* gene encodes the Rho family GTPase Rho5, which is localized to the terminal end of interphase cells and the intermediate region of mitotic cells and participates in the regulation of the actin cytoskeletal organization and the synthesis of the cell wall (65). The *wos2* gene encodes the p23 homolog, the Hsp90 co-chaperone Wos2, which is involved in the regulation of protein-containing complex assembly, and deletion of the *wos2* gene results in cell lysis and abnormal mitotic cell cycle (15). The anaphase-promoting complex subunit Apc14 is involved in anaphase-promoting complex-dependent catabolic process and mitotic sister chromatid segregation, and *apc14* gene deletion results in reduced mitotic checkpoint complex binding (66,67). The downregulation of *apc14* may account for the delayed separation of centromeres during mitosis in the *rok1*Δ strain at 37˚C in this study. This suggests that the Rok1 protein may influence the ability of centromeres to migrate along the spindle.

The *arp1* gene encodes the dynactin complex subunit, the centractin family actin-like protein Arp1. In *S. pombe*, Arp1, Mug5 and Jnm1 constitute core components of the dynactin complex, with Arp1 localizing to dynein anchoring sites at the cell cortex. Arp1, Mug5, Jnm1 and the dynactin microtubule-binding subunit Ssm4, which interacts with

Mug5, participate in dynein anchoring and regulation of microtubule contraction. Deletion of the *arp1* gene results in reduced microtubule depolymerization rates (68). The *dli1* gene encodes the meiotic dynein intermediate light chain Dli1, which facilitates the increased expression of the dynein complex core molecule Dhc1. This enhancement promotes the binding of dynein to both the spindle pole body (SPB) and microtubules (MTs), thereby facilitating MT elongation (69). The *mfr1* gene encodes the meiotic APC activator Mfr1; Mfr1 binds to the meiosis-specific protein Mes1, and its expression can rescue the entry defect at meiosis II in *mes1*Δ cells (70). Additionally, Mfr1 mediates the rapid degradation of Cdc13 cyclin at the end of meiosis II, ensuring proper exit from meiosis. Mfr1 null mutants complete meiosis II but maintain high levels of Cdc13 and Cdc2 kinase activity, resulting in delayed exit from cell division (71). The *cmk1* gene encodes the Ca^{2+}/calmodulin-dependent kinase Cmk1; Cmk1 phosphorylates the M-phase inducer Cdc25 phosphatase, regulating Cdk1 activity, and levels are closely associated with spindle dynamics: During metaphase when Cdk1 activity is high, the microtubule site clamping complex subunit Mde4 is phosphorylated at its Cdk1 phosphorylation sites and localizes to kinetochores; during anaphase, decreased Cdk1 activity leads to Mde4 dephosphorylation and translocation to the spindle, promoting spindle elongation and maintaining its integrity (72). Furthermore, *cmk1* gene expression was downregulated in *rok1*Δ cells at 37˚C, accompanied by shortened spindle elongation length and reduced centromere separation distance. However, RNA-Seq revealed no differential expression of centromere-related genes, with changes only detected in genes involved in the microtubule assembly pathway, such as *cmk1*. These results indicate that although prominent phenotypic alterations were observed at the centromere level, the underlying cause likely does not originate from aberrant expression of centromere-associated proteins. The findings suggest that Rok1 more plausibly influences centromere phenotypic variation indirectly by modulating the microtubule assembly process, in which Cmk1 appears to serve a representative role.

KEGG, as a systematic pathway database, provides standardized biological pathway annotations and enrichment analysis for differentially expressed genes, serving as a core tool for deciphering the molecular mechanisms underlying high-throughput data (38). Cell cycle regulation is a process required to ensure the maintenance of genome integrity, and mitotic abnormalities caused by cell cycle dysregulation trigger autophagy through various protein interactions. Autophagy combines cell growth with cell division to maintain the integrity of the nuclear and mitochondrial genomes. Defective autophagy leads to defective cell growth and is associated with abnormal mitosis (73). At 25˚C, in the cell cycle-yeast pathway, the Spo4 protein has protein serine/threonine kinase activity and is involved in the reorganization of specific spindle pole bodies during meiosis, regulating ascospore formation; Spo4 protein deficiency results in abnormal prospore membrane formation and chromosome segregation (23,74). The *rad17* gene encodes the replication factor C-related checkpoint protein Rad17, which is localized in the nucleus by binding to chromatin; Rad17 is involved in regulating mitotic DNA replication checkpoint and DNA damage checkpoint signaling in G_2 phase (75). The *mad1* gene encodes the mitotic spindle checkpoint protein Mad1, which recruits Cut7 proteins to the mismatched kinetochore in chromosomes, promotes chromosome sliding on the spindle and is involved in the mitotic spindle assembly checkpoint signaling process (76). The *psm1* gene encodes the ATPase subunit Psm1 of the mitotic/meiotic cohesin complex, which participates in establishing sister chromatid cohesion during mitosis. The Psm1-Psm3 head domain heterodimer, Mis4 and the N-terminal helical domain of Rec8 bound to the coiled-coil region of Psm3 collectively form the primary chromatin-binding region of the cohesin complex. By recruiting Plo1 kinase, this complex promotes the phosphorylation of Rec8, thereby ensuring the mono-orientation of sister kinetochores (77,78). The cohesin loading factor (adherin) Mis4/Scc2, which has ATPase activator activity, forms a tertiary complex with cohesins on DNA and is involved in the regulation of mitotic sister chromatid cohesion and chromosome segregation. Abnormalities in the Mis4 protein lead to abnormal cell cycle arrest and premature sister chromatid segregation in mitosis (79,80). Abnormal expression of cell cycle pathway genes suggested that the cytokinesis process was affected in the *rok1*Δ-25˚C strain. This was consistent with the abnormal results of spore formation and mitosis in the *rok1*Δ-25˚C strain, and with the results of GO enrichment analysis (Fig. 9).

At 37˚C, the autophagy-yeast pathway, the *pas1* gene encodes the cell cycle protein Pas1, which is involved in the composition of the cyclin-dependent protein kinase holoenzyme complex that negatively regulates the mitotic cell cycle G_1/S transition and sister chromatid cohesion (64). Atg17 participates in cellular autophagosome assembly as an autophagy associated protein kinase activator to remove its own damaged cellular structures; deletion of Atg17 results in a decreased sporulation frequency and an abnormal G_1 to G_0 transition (81,82). Atg13 is co-localized with other Atg machinery proteins at the phagocytic vesicle assembly site in the proximal endoplasmic reticulum and is involved in cellular autophagosome assembly; *atg13* gene deletion results in abnormal spore formation and autophagy processes (83). The *atg15* gene encodes the autophagy-associated lysophospholipase Atg15, which is involved in the regulation of microautophagy of the nucleus. Chromosome segregation and cellular autophagy are abnormal in *atg15*Δ strains, and the frequency of spore formation is decreased (23,83). The *arc1* gene encodes the Arp2/3 actin organizing complex WD repeat subunit Sop2, which is involved in the composition of the Arp2/3 protein complex to mediate actin polymerization; aberrant Sop2 protein decreases protein localization to actomyosin contractile ring during mitosis (84). Abnormal expression of the autophagy pathway indicated impaired mitotic processes in the *rok1*Δ-37˚C strain. This was consistent with the abnormal results of actin formation and contraction and kinetochore separation in the *rok1*Δ-37˚C strain, as well as with the results of GO enrichment analysis. In addition, although the ribosomal pathway was upregulated in both *rok1*Δ-25˚C and *rok1*Δ-37˚C strains, few genes were

upregulated in both. Therefore, *rok1* gene deletion mainly regulated the mitotic process through up- and downregulation of different pathways at 25 and 37˚C.

Temperature is a critical factor influencing protein synthesis and function in cells. In the present study, two culture temperatures, 25 and 37˚C, were selected to investigate the potential biological functions of the *rok1* gene deletion under heat stress to amplify the phenotypic effects results. This experimental approach has been widely adopted in related studies; for instance, Codlin *et al* (85) discovered that btn1-deficient cells exhibited only mild proliferation defects under normal growth conditions at 25˚C, whereas severe depolarization and cell lysis were observed under heat stress at 37˚C. This revealed the role of Btn1p in the F-actin-dependent endocytosis-polarized growth coupling pathway. Similarly, Hoya *et al* (86) identified functional overlap between exomer and GGA22 by analyzing the synthetic growth defects of the *gga22*Δ *cfr1*Δ double mutant under both low-temperature (22˚C) and high-temperature (36˚C) stress conditions. It is important to note that phenotypic variations in strains at different temperatures are a common phenomenon and are generally not defined as temperature-sensitive strains. Temperature-sensitive strains specifically refer to those that exhibit complete growth arrest or total loss of protein function at a restrictive temperature (87). Such strains show 100% growth inhibition under non-permissive conditions; therefore, the *rok1*Δ strain investigated here is not a temperature-sensitive strain.

Notably, no widespread ribosome biosynthesis dysfunction was observed in the *rok1*Δ strain in the present study; mitotic progression remained normal and transcriptomic analysis did not reveal a global decline in protein translation levels. Instead, only specific alterations in the expression of actin-related proteins were detected. Based on comprehensive review of literature on the *rok1* gene in fission yeast, to the best of our knowledge, there is currently no evidence indicating that *rok1* directly affects protein translation through ribosome biosynthesis. Therefore, the present study proposes a novel mechanism: The decreased translation levels of actin-related proteins represent a direct consequence of *rok1* deletion, rather than being secondary to ribosome biogenesis defects, revealing a previously unrecognized role of the *rok1* gene in mitotic dynamics.

Currently, research on the *rok1* gene in fission yeast has primarily focused on its role in ribosome biogenesis, while its mechanism in regulating mitotic dynamics remains unclear. There is a particular lack of studies investigating the effects of rok1 deletion on mitosis and its molecular mechanisms under both normal and stress temperature conditions. Using fission yeast as a model, the present study demonstrated that *rok1* deletion leads to slow cell growth, abnormal spore numbers, shortened spindles and centromere separation distance, delayed actin ring assembly and blocked migration of the kinetochores on the spindle. Integrated RNA-Seq and bioinformatics analyses suggest that the Rok1 protein regulates actin polymerization, thereby participating in actin ring assembly, contraction and cytokinesis, while potentially influencing kinetochore mobility on the spindle or contributing to the establishment and maintenance of sister chromatid cohesion. Notably, this novel function of Rok1 appears independent of its canonical RNA helicase activity and may instead be linked to differential expression of genes such as *myo51*, *blt1*, *psm1* and *psc3* in *rok1*Δ cells.

The present study preliminarily reveals potential functional associations between *rok1* and these differentially expressed genes. However, the specific interaction relationships and regulatory mechanisms have not yet been directly validated at the protein level, which represents a major limitation of the current research. To further clarify the roles of these genes within the Rok1 regulatory network, subsequent plans involve screening key target genes through overexpression or knockout experiments combined with phenotypic analysis. Building upon this foundation, in-depth studies on protein interactions and functional validation will be conducted.

Acknowledgements

The authors would like to acknowledge Associate Professor Phong Tran (Department of Cell and Developmental Biology, University of Pennsylvania) for donating the yeast strains.

Funding

The present study was funded by the Sichuan Province Science and Technology Support Project (grant nos. 2022NZZJ0003, 22ZYZFSF0009, 2022NSFSC0107 and 23ZHSF0082).

Availability of data and materials

The transcriptome data in the present study have been deposited in the CNCB and NCBI databases under BioProject accession numbers PRJCA051218, https://ngdc.cncb.ac.cn/bioproject/browse/PRJCA051218 and PRJNA1208695, https://www.ncbi.nlm.nih.gov/bioproject/PRJNA1208695/. All other data presented in the present study may be requested from the corresponding author.

Authors' contributions

YH and XD conceived and designed the experiments of the present study. JH, ML and JX performed the experiments and analyzed the data. JH, ML, JX and XD drafted the manuscript and revised it critically. All authors read approved the final version of the manuscript. JH and ML confirm the authenticity of all the raw data.

Ethics approval and consent to participate

Not applicable.

Patient consent for publication

Not applicable.

Competing interests

The authors declare that they have no competing interests.

References

1. Cho RJ, Campbell MJ, Winzeler EA, Steinmetz L, Conway A, Wodicka L, Wolfsberg TG, Gabrielian AE, Landsman D, Lockhart DJ and Davis RW: A genome-wide transcriptional analysis of the mitotic cell cycle. Mol Cell 2: 65-73, 1998.
2. Cook BD, Chang F, Flor-Parra I and Al-Bassam J: Microtubule polymerase and processive plus-end tracking functions originate from distinct features within TOG domain arrays. Mol Biol Cell 30: 1490-1504, 2019.
3. Plastino J and Blanchoin L: Dynamic stability of the actin ecosystem. J Cell Sci 132: jcs219832, 2018.
4. Nema R and Kumar A: BUB1, miR-495-3p, and E2F1/E2F8 axis is associated with poor prognosis of breast cancer patients and infiltration of Th2 cells in the tumor microenvironment. Cancer Biomark 42: 18758592241310109, 2025.
5. Chu A, Liu X, Liu S, Li M, Song R, Gan L, Wang Y, Liu Z and Sun C: RNA-seq analysis reveals key genes associated with downregulation of APE1 in esophageal squamous cell carcinoma. Front Genet 16: 1549371, 2025.
6. McInerny CJ: Cell cycle regulated gene expression in yeasts. Adv Genet 73: 51-85, 2011.
7. Wang L, Chen K, Weng S, Xu H, Ren Y, Cheng Q, Luo P, Zhang J, Liu Z and Han X: PI3K pathway mutation predicts an activated immune microenvironment and better immunotherapeutic efficacy in head and neck squamous cell carcinoma. World J Surg Oncol 21: 72, 2023.
8. Vejrup-Hansen R, Mizuno K, Miyabe I, Fleck O, Holmberg C, Murray JM, Carr AM and Nielsen O: *Schizosaccharomyces pombe* Mms1 channels repair of perturbed replication into Rhp51 independent homologous recombination. DNA Repair (Amst) 10: 283-295, 2011.
9. MacQuarrie CD, Mangione MC, Carroll R, James M, Gould KL and Sirotkin V: The *S. pombe* adaptor protein Bbc1 regulates localization of Wsp1 and Vrp1 during endocytic actin patch assembly. J Cell Sci 132: jcs233502, 2019.
10. Szkotnicki L, Crutchley JM, Zyla TR, Bardes ESG and Lew DJ: The checkpoint kinase Hsl1p is activated by Elm1p-dependent phosphorylation. Mol Biol Cell 19: 4675-4686, 2008.
11. Grallert B, Kearsey SE, Lenhard M, Carlson CR, Nurse P, Boye E and Labib K: A fission yeast general translation factor reveals links between protein synthesis and cell cycle controls. J Cell Sci 113: 1447-1458, 2000.
12. Johnson CA, Brooker HR, Gyamfi I, O'Brien J, Ashley B, Brazier JE, Dean A, Embling J, Grimsey E, Tomlinson AC, *et al*: Temperature sensitive point mutations in fission yeast tropomyosin have long range effects on the stability and function of the actin-tropomyosin copolymer. Biochem Biophys Res Commun 506: 339-346, 2018.
13. Karbstein K: Attacking a DEAD problem: The role of DEAD-box ATPases in ribosome assembly and beyond. Methods Enzymol 673: 19-38, 2022.
14. Dudin O, Merlini L, Bendezú FO, Groux R, Vincenzetti V and Martin SG: A systematic screen for morphological abnormalities during fission yeast sexual reproduction identifies a mechanism of actin aster formation for cell fusion. PLoS Genet 13: e1006721, 2017.
15. Hayles J, Wood V, Jeffery L, Hoe KL, Kim DU, Park HO, Salas-Pino S, Heichinger C and Nurse P: A genome-wide resource of cell cycle and cell shape genes of fission yeast. Open Biol 3: 130053, 2013.
16. Maekawa H, Nakagawa T, Uno Y, Kitamura K and Shimoda C: The ste13+ gene encoding a putative RNA helicase is essential for nitrogen starvation-induced G1 arrest and initiation of sexual development in the fission yeast *Schizosaccharomyces pombe*. Mol Gen Genet 244: 456-464, 1994.
17. Forbes KC, Humphrey T and Enoch T: Suppressors of cdc25p overexpression identify two pathways that influence the G2/M checkpoint in fission yeast. Genetics 150: 1361-1375, 1998.
18. Ren L, McLean JR, Hazbun TR, Fields S, Vander Kooi C, Ohi MD and Gould KL: Systematic two-hybrid and comparative proteomic analyses reveal novel yeast pre-mRNA splicing factors connected to Prp19. PLoS One 6: e16719, 2011.
19. Potashkin J, Kim D, Fons M, Humphrey T and Frendewey D: Cell-division-cycle defects associated with fission yeast pre-mRNA splicing mutants. Curr Genet 34: 153-163, 1998.
20. Linder P and Jankowsky E: From unwinding to clamping-the DEAD box RNA helicase family. Nat Rev Mol Cell Biol 12: 505-516, 2011.
21. Khoshnevis S, Askenasy I, Johnson MC, Dattolo MD, Young-Erdos CL, Stroupe ME and Karbstein K: The DEAD-box protein Rok1 orchestrates 40S and 60S ribosome assembly by promoting the release of Rrp5 from Pre-40S ribosomes to allow for 60S maturation. PLoS Biol 14: e1002480, 2016.
22. Jeon S, Lim S, Ha J and Kim J: Identification of Psk2, Skp1, and Tub4 as trans-acting factors for uORF-containing ROK1 mRNA in Saccharomyces cerevisiae. J Microbiol 53: 616-622, 2015.
23. Blyth J, Makrantoni V, Barton RE, Spanos C, Rappsilber J and Marston AL: Genes important for *Schizosaccharomyces pombe* meiosis identified through a functional genomics screen. Genetics 208: 589-603, 2018.
24. Lin SL, Chang D and Ying SY: Hyaluronan stimulates transformation of androgen-independent prostate cancer. Carcinogenesis 28: 310-320, 2007.
25. Zhang D, Yu W, Liu M, Qing X, Ding X and Hou Y: Effects of the mitochondrial fission gene dnm1 deletion on mitosis and energy metabolism in Saccharomyces cerevisiae cells. J Beijing Normal Univ 60: 331-343, 2024.
26. Yu W, Yuan R, Liu M, Liu K, Ding X and Hou Y: Effects of rpl1001 gene deletion on cell division of fission yeast and its molecular mechanism. Curr Issues Mol Biol 46: 2576-2597, 2024.
27. Furuya K and Niki H: Mating, spore dissection, and selection of diploid cells in *Schizosaccharomyces japonicus*. Cold Spring Harb Protoc 2017: prot091843, 2017.
28. Hu Z, Chen C, Zheng X, Yuan J, Zou R and Xie C: Establishing gene expression and knockout methods in esteya vermicola CBS115803. Mol Biotechnol 66: 2872-2881, 2024.
29. Lai CJS, Tan T, Zeng SL, Xu LR, Qi LW, Liu EH and Li P: An enzymatic protocol for absolute quantification of analogues: Application to specific protopanoxadiol-type ginsenosides. Green Chem 17: 2580-2586, 2015.
30. Brown SD and Lorenz A: Single-step marker switching in *Schizosaccharomyces pombe* using a lithium acetate transformation protocol. Bio Protoc 6: e2075, 2016.
31. DeVore GR: Computing the Z score and centiles for cross-sectional analysis: A practical approach. J Ultrasound Med 36: 459-473, 2017.
32. Katz Y, Wang ET, Airoldi EM and Burge CB: Analysis and design of RNA sequencing experiments for identifying isoform regulation. Nat Methods 7: 1009-1015, 2010.
33. Hampton TH, Taub L, Ferreria-Fukutani K, Stanton BA and MacKenzie TA: Analyzing qPCR data: Better practices to facilitate rigor and reproducibility. Biochem Biophys Rep 44: 102356, 2025.
34. Kim D, Paggi JM, Park C, Bennett C and Salzberg SL: Graph-based genome alignment and genotyping with HISAT2 and HISAT-genotype. Nat Biotechnol 37: 907-915, 2019.
35. Liao Y, Smyth GK and Shi W: featureCounts: An efficient general purpose program for assigning sequence reads to genomic features. Bioinformatics 30: 923-930, 2014.
36. Liu S, Wang Z, Zhu R, Wang F, Cheng Y and Liu Y: Three differential expression analysis methods for RNA sequencing: limma, EdgeR, DESeq2. J Vis Exp, 2021.
37. Ashburner M, Ball CA, Blake JA, Botstein D, Butler H, Cherry JM, Davis AP, Dolinski K, Dwight SS, Eppig JT, *et al*: Gene ontology: Tool for the unification of biology. The gene ontology consortium. Nat Genet 25: 25-29, 2000.
38. Ogata H, Goto S, Sato K, Fujibuchi W, Bono H and Kanehisa M: KEGG: Kyoto encyclopedia of genes and genomes. Nucleic Acids Res 27: 29-34, 1999.
39. Yu G, Wang LG, Han Y and He QY: clusterProfiler: An R package for comparing biological themes among gene clusters. OMICS 16: 284-287, 2012.
40. Brown SD, Audoynaud C and Lorenz A: Intragenic meiotic recombination in *Schizosaccharomyces pombe* is sensitive to environmental temperature changes. Chromosome Res 28: 195-207, 2020.
41. Nunes V and Ferreira JG: From the cytoskeleton to the nucleus: An integrated view on early spindle assembly. Semin Cell Dev Biol 117: 42-51, 2021.
42. Rezig IM, Yaduma WG and McInerny CJ: Processes controlling the contractile ring during cytokinesis in fission yeast, including the role of ESCRT proteins. J Fungi (Basel) 10: 154, 2024.
43. Goldstein LD, Cao Y, Pau G, Lawrence M, Wu TD, Seshagiri S and Gentleman R: Prediction and quantification of splice events from RNA-Seq data. PLoS One 11: 156132, 2016.
44. Zhao Y, Li MC, Konaté MM, Chen L, Das B, Karlovich C, Williams PM, Evrard YA, Doroshow JH and McShane LM: TPM, FPKM, or normalized counts? A comparative study of quantification measures for the analysis of RNA-seq data from the NCI patient-derived models repository. J Transl Med 19: 269, 2021.

45. Morigasaki S, Shimada K, Ikner A, Yanagida M and Shiozaki K: Glycolytic enzyme GAPDH promotes peroxide stress signaling through multistep phosphorelay to a MAPK cascade. Mol Cell 30: 108-113, 2008.
46. Zhang Y and Barberis M: Exploring cell cycle-mediated regulations of glycolysis in budding yeast. Front Microbiol 14: 1270487, 2023.
47. Boronat S, Domènech A, Carmona M, García-Santamarina S, Bañó MC, Ayté J and Hidalgo E: Lack of a peroxiredoxin suppresses the lethality of cells devoid of electron donors by channelling electrons to oxidized ribonucleotide reductase. PLoS Genet 13: e1006858, 2017.
48. Matsuyama A, Arai R, Yashiroda Y, Shirai A, Kamata A, Sekido S, Kobayashi Y, Hashimoto A, Hamamoto M, Hiraoka Y, *et al*: ORFeome cloning and global analysis of protein localization in the fission yeast *Schizosaccharomyces pombe*. Nat Biotechnol 24: 841-847, 2006.
49. Xiang B, Chen ML, Gao ZQ, Mi T, Shi QL, Dong JJ, Tian XM, Liu F and Wei GH: CCNB1 is a novel prognostic biomarker and promotes proliferation, migration and invasion in Wilms tumor. BMC Med Genomics 16: 189, 2023.
50. Otsubo Y, Yamashita A, Ohno H and Yamamoto M: *S. pombe* TORC1 activates the ubiquitin-proteasomal degradation of the meiotic regulator Mei2 in cooperation with Pat1 kinase. J Cell Sci 127: 2639-2646, 2014.
51. Sasuga S, Abe R, Nikaido O, Kiyosaki S, Sekiguchi H, Ikai A and Osada T: Interaction between pheromone and its receptor of the fission yeast *Schizosaccharomyces* pombe examined by a force spectroscopy study. J Biomed Biotechnol 2012: 804793, 2012.
52. Miyata M, Matsuoka M and Inada T: Induction of sexual co-flocculation of heterothallic fission yeast (*Schizosaccharomyces pombe*) cells by mating pheromones. J Gen Appl Microbiol 43: 169-174, 1997.
53. Imai Y and Yamamoto M: The fission yeast mating pheromone P-factor: Its molecular structure, gene structure, and ability to induce gene expression and G1 arrest in the mating partner. Genes Dev 8: 328-338, 1994.
54. Ilyushik E, Pryce DW, Walerych D, Riddell T, Wakeman JA, McInerny CJ and McFarlane RJ: Psc3 cohesin of *Schizosaccharomyces pombe*: Cell cycle analysis and identification of three distinct isoforms. Biol Chem 386: 613-621, 2005.
55. Pereira G and Schiebel E: The role of the yeast spindle pole body and the mammalian centrosome in regulating late mitotic events. Curr Opin Cell Biol 13: 762-769, 2001.
56. Merlini L, Khalili B, Dudin O, Michon L, Vincenzetti V and Martin SG: Inhibition of Ras activity coordinates cell fusion with cell-cell contact during yeast mating. J Cell Biol 217: 1467-1483, 2018.
57. Tang Q, Billington N, Krementsova EB, Bookwalter CS, Lord M and Trybus KM: A single-headed fission yeast myosin V transports actin in a tropomyosin-dependent manner. J Cell Biol 214: 167-179, 2016.
58. Wang N, Lo Presti L, Zhu YH, Kang M, Wu Z, Martin SG and Wu JQ: The novel proteins Rng8 and Rng9 regulate the myosin-V Myo51 during fission yeast cytokinesis. J Cell Biol 205: 357-375, 2014.
59. Tyree ZL, Bellingham-Johnstun K, Martinez-Baird J and Laplante C: The myosin-V Myo51 and alpha-actinin Ain1p cooperate during contractile ring assembly and disassembly in fission yeast cytokinesis. J Fungi (Basel) 10: 647, 2024.
60. Win TZ, Gachet Y, Mulvihill DP, May KM and Hyams JS: Two type V myosins with non-overlapping functions in the fission yeast *Schizosaccharomyces pombe*: Myo52 is concerned with growth polarity and cytokinesis, Myo51 is a component of the cytokinetic actin ring. J Cell Sci 114: 69-79, 2001.
61. Laplante C, Berro J, Karatekin E, Hernandez-Leyva A, Lee R and Pollard TD: Three myosins contribute uniquely to the assembly and constriction of the fission yeast cytokinetic contractile ring. Curr Biol 25: 1955-1965, 2015.
62. Goss JW, Kim S, Bledsoe H and Pollard TD: Characterization of the roles of Blt1p in fission yeast cytokinesis. Mol Biol Cell 25: 1946-1957, 2014.
63. Jourdain I, Brzezińska EA and Toda T: Fission yeast Nod1 is a component of cortical nodes involved in cell size control and division site placement. PLoS One 8: e54142, 2013.
64. Birot A, Tormos-Pérez M, Vaur S, Feytout A, Jaegy J, Alonso Gil D, Vazquez S, Ekwall K and Javerzat JP: The CDK Pef1 and protein phosphatase 4 oppose each other for regulating cohesin binding to fission yeast chromosomes. Elife 9: e50556, 2020.
65. Nakano K, Arai R and Mabuchi I: Small GTPase Rho5 is a functional homologue of Rho1, which controls cell shape and septation in fission yeast. FEBS Lett 579: 5181-5186, 2005.
66. Yoon HJ, Feoktistova A, Wolfe BA, Jennings JL, Link AJ and Gould KL: Proteomics analysis identifies new components of the fission and budding yeast anaphase-promoting complexes. Curr Biol 12: 2048-2054, 2002.
67. May KM, Paldi F and Hardwick KG: Fission yeast Apc15 stabilizes MCC-Cdc20-APC/C complexes, ensuring efficient Cdc20 ubiquitination and checkpoint arrest Curr Biol 27: 1221-1228, 2017.
68. Fujita I, Yamashita A and Yamamoto M: Dynactin and Num1 cooperate to establish the cortical anchoring of cytoplasmic dynein in *S. pombe*. J Cell Sci 128: 1555-1567, 2015.
69. Scheffler K, Minnes R, Fraisier V, Paoletti A and Tran PT: Microtubule minus end motors kinesin-14 and dynein drive nuclear congression in parallel pathways. J Cell Biol 209: 47-58, 2015.
70. Kimata Y, Kitamura K, Fenner N and Yamano H: Mes1 controls the meiosis I to meiosis II transition by distinctly regulating the anaphase-promoting complex/cyclosome coactivators Fzr1/Mfr1 and Slp1 in fission yeast. Mol Biol Cell 22: 1486-1494, 2011.
71. Blanco MA, Pelloquin L and Moreno S: Fission yeast mfr1 activates APC and coordinates meiotic nuclear division with sporulation. J Cell Sci 114: 2135-2143, 2001.
72. Gregan J, Riedel CG, Pidoux AL, Katou Y, Rumpf C, Schleiffer A, Kearsey SE, Shirahige K, Allshire RC and Nasmyth K: The kinetochore proteins Pcs1 and Mde4 and heterochromatin are required to prevent merotelic orientation. Curr Biol 17: 1190-1200, 2007.
73. Azzopardi M, Farrugia G and Balzan R: Cell-cycle involvement in autophagy and apoptosis in yeast. Mech Ageing Dev 161: 211-224, 2017.
74. Ucisik-Akkaya E, Leatherwood JK and Neiman AM: A genome-wide screen for sporulation-defective mutants in *Schizosaccharomyces pombe*. G3 (Bethesda) 4: 1173-1182, 2014.
75. al-Khodairy F, Fotou E, Sheldrick KS, Griffiths DJ, Lehmann AR and Carr AM: Identification and characterization of new elements involved in checkpoint and feedback controls in fission yeast. Mol Biol Cell 5: 147-160, 1994.
76. Akera T, Goto Y, Sato M, Yamamoto M and Watanabe Y: Mad1 promotes chromosome congression by anchoring a kinesin motor to the kinetochore. Nat Cell Biol 17: 1124-1133, 2015.
77. Tomonaga T, Nagao K, Kawasaki Y, Furuya K, Murakami A, Morishita J, Yuasa T, Sutani T, Kearsey SE, Uhlmann F, *et al*: Characterization of fission yeast cohesin: Essential anaphase proteolysis of Rad21 phosphorylated in the S phase. Genes Dev 14: 2757-2770, 2000.
78. Liu Y, Min Y, Liu Y and Watanabe Y: Phosphorylation of Rec8 cohesin complexes regulates mono-orientation of kinetochores in meiosis I. Life Sci Alliance 7: e202302556, 2024.
79. Kurokawa Y and Murayama Y: DNA binding by the $Mis4^{Scc2}$ loader promotes topological DNA entrapment by the cohesin ring. Cell Rep 33: 108357, 2020.
80. Furuya K, Takahashi K and Yanagida M: Faithful anaphase is ensured by Mis4, a sister chromatid cohesion molecule required in S phase and not destroyed in G1 phase. Genes Dev 12: 3408-3418, 1998.
81. Zhao D, Liu XM, Yu ZQ, Sun LL, Xiong X, Dong MQ and Du LL: Atg20- and Atg24-family proteins promote organelle autophagy in fission yeast. J Cell Sci 129: 4289-4304, 2016.
82. Zahedi Y, Durand-Dubief M and Ekwall K: High-throughput flow cytometry combined with genetic analysis brings new insights into the understanding of chromatin regulation of cellular quiescence. Int J Mol Sci 21: 9022, 2020.
83. Mukaiyama H, Kajiwara S, Hosomi A, Giga-Hama Y, Tanaka N, Nakamura T and Takegawa K: Autophagy-deficient *Schizosaccharomyces pombe* mutants undergo partial sporulation during nitrogen starvation. Microbiology (Reading) 155: 3816-3826, 2009.
84. Balasubramanian MK, Feoktistova A, McCollum D and Gould KL: Fission yeast Sop2p: A novel and evolutionarily conserved protein that interacts with Arp3p and modulates profilin function. EMBO J 15: 6426-6437, 1996.
85. Codlin S, Haines RL, and Mole SE: btn1 affects endocytosis, polarization of cholesterol-enriched membrane domains, and polarized growth in Schizosaccharomyces pombe. Traffic 9: 936-950, 2008.